

1 **Measurement report: Enhanced photochemical formation of**
2 **formic and isocyanic acids in urban region aloft: insights**
3 **from tower-based online gradient measurements**

4 Qing Yang^{1,2}, Xiao-Bing Li^{1,2,*}, Bin Yuan^{1,2,*}, Xiaoxiao Zhang^{1,2}, Yibo Huangfu^{1,2}, Lei
5 Yang^{1,2}, Xianjun He^{1,2}, Jipeng Qi^{1,2}, Min Shao^{1,2}

6 ¹ Institute for Environmental and Climate Research, Jinan University, Guangzhou
7 511443, China

8 ² Guangdong-Hongkong-Macau Joint Laboratory of Collaborative Innovation for
9 Environmental Quality, Guangzhou 511443, China

10 * Corresponding authors: Xiao-Bing Li (lixiaobing@jnu.edu.cn), Bin Yuan
11 (byuan@jnu.edu.cn)

12 **Abstract**

13 Formic acid is the most abundant organic acid in the troposphere and has
14 significant environmental and climatic impacts. Isocyanic acid poses severe threats to
15 human health and could be formed through the degradation of formic acid. However,
16 the lack of vertical observation information has strongly limited the understanding of
17 their sources, particularly in urban regions with complex pollutant emissions. To
18 address this issue, we assessed the impact of long tubes on the measurement
19 uncertainties of formic and isocyanic acids and found that the tubing impact was
20 negligible. Then, we conducted continuous (27 days) vertical gradient measurements
21 (five heights between 5-320 m) of formic and isocyanic acids using long tubes based
22 on a tall tower in Beijing, China, in the summer of 2021. Results show that the
23 respective mean mixing ratios of formic and isocyanic acids were 1.3 ± 1.3 ppbv and
24 0.28 ± 0.16 ppbv at 5 m and were 2.1 ± 1.9 ppbv and 0.43 ± 0.21 ppbv at 320 m during the
25 campaign. The mixing ratios of formic and isocyanic acids were substantially enhanced
26 in daytime and correlated with the diurnal change of ozone. Upon sunrise, the mixing
27 ratios of formic and isocyanic acids at different heights simultaneously increased even
28 in the residual layer. In addition, positive vertical gradients were observed for formic
29 and isocyanic acids throughout the day. The positive vertical gradients of formic and
30 isocyanic acids in daytime imply the enhancement of their secondary formation in
31 urban regions aloft, predominantly due to the enhancements of oxygenated volatile
32 organic compounds. Furthermore, the afternoon peaks and positive vertical gradients
33 of formic and isocyanic acids in nighttime also indicate their minor contributions from
34 primary emissions from ground-level sources. The formation pathway of isocyanic acid
35 through $\text{HCOOH}-\text{CH}_3\text{NO}-\text{HNCO}$ was enhanced with height but only accounted for a
36 tiny fraction of its ambient abundance. The abundance and source contributions of
37 formic and isocyanic acids in the atmospheric boundary layer may be highly
38 underestimated when being derived from their ground-level measurements. With the
39 aid of numerical modeling techniques, future studies could further identify key

40 precursors that drive the rapid formation of formic and isocyanic acids, and
41 quantitatively assess the impacts of the enhanced formation of the two acids aloft on
42 their budgets at ground level.

43 **1. Introduction**

44 Formic acid (HCOOH) is the simplest but the most abundant organic acid in the
45 troposphere. It has been widely measured in aqueous (clouds and aerosols) and gaseous
46 phases over urban, rural, and remote regions (*Kawamura and Kaplan, 1983; Chebbi
47 and Carlier, 1996; Kesselmeier et al., 1998; Yu, 2000*). As important contributors to the
48 acidity of precipitation, formic and acetic acids can account for 60% of the free acidity
49 in remote regions (*Galloway et al., 1982; Andreae et al., 1988*), and over 30% of the
50 free acidity in heavily polluted regions (*Keene and Galloway, 1984*). Formic acid is
51 also an important sink of hydroxyl radicals (OH) in clouds (*Jacob, 1986*), playing vital
52 roles in modulating the atmospheric aqueous-phase chemistry through changing pH-
53 dependent reaction rates of related constituents. An in-depth understanding of the
54 concentration levels, spatiotemporal variations, and sources of formic acid is key to
55 elucidating the formation mechanisms of atmospheric secondary pollution. However,
56 the sources and sinks of atmospheric formic acid are still poorly understood so far.

57 There have been many reported sources of atmospheric formic acid. Primary
58 emissions from vegetation activity (*Andreae et al., 1988; Kesselmeier et al., 1998*),
59 microbial metabolism (*Enders et al., 1992*), biomass burning (*Goode et al., 2000*), and
60 vehicle exhaust (*Kawamura et al., 2000*) were identified as important sources of formic
61 acid. Secondary formation from photochemical degradation of volatile organic
62 compounds (VOCs) is another significant source of formic acid (*Khare et al., 1999;
63 Veres et al., 2011; Le Breton et al., 2014; Liggio et al., 2017*). However, current
64 chemical transport models still highly underestimate ambient concentrations of formic
65 acid (*Stavrakou et al., 2011; Paulot et al., 2011; Millet et al., 2015*) and cannot well
66 reproduce its vertical variations. For example, *Mattila et al. (2018)* measured vertical
67 profiles of formic acid using an elevator on the Colorado Front Range BOA tower. They
68 found that formic acid mixing ratios generally decreased with height throughout the day,
69 but there were no known sources to explicitly explain the net surface emissions. In
70 combination with vertical gradient and flux measurements of formic acid in a forest

71 ecosystem, Alwe et al. (2019) suggested that secondary formation, rather than primary
72 emission, is the major source of ambient formic acid. The vertical distribution and
73 variation patterns of formic acid in the atmospheric boundary layer can provide
74 valuable information on the identification and determination of source contributions.
75 Nevertheless, the vertical variations and key drivers of formic acid, particularly in urban
76 regions, are still unclear due to the lack of adequate vertical observations.

77 Isocyanic acid (HNCO) is an inorganic acid and has attracted extensive concerns
78 worldwide in recent years due to its strong toxicity (Wang et al., 2007; Jaisson et al.,
79 2011; Koeth et al., 2013). Previous studies have reported that isocyanic acid is highly
80 soluble at physiological pH and the dissociated cyanate ions (NCO^-) are closely linked
81 to atherosclerosis, cataracts, and rheumatoid arthritis (Mydel et al., 2010; Roberts et al.,
82 2011). At present, there is no standard to clearly define the critical levels of isocyanic
83 acid pollution in ambient air (Rosanka et al., 2020). The mixing ratio of HNCO in the
84 atmosphere exceeding 1 ppbv may endanger human health (Roberts et al., 2011), and
85 the protein carbamylation caused by HNCO in human body may induce various risks
86 (Verbrugge et al., 2015). Similar to formic acid, our understanding of isocyanic acid
87 sources is also very limited.

88 As reported in the literature, primary emissions of isocyanic acid are mainly from
89 combustion sources including cigarette smoke (Hems et al., 2019), gasoline and diesel
90 engine exhausts (Wren et al., 2018), and biomass combustion (Wentzell et al., 2013; Li
91 et al., 2021; Chandra and Sinha, 2016). Wet and dry deposition is known as the main
92 sink of isocyanic acid (Roberts et al., 2014; Rosanka et al., 2020). In addition, isocyanic
93 acid is highly soluble at atmospheric pH and can be hydrolyzed to NH_3 and CO_2 (Zhao
94 et al., 2014; Roberts and Liu, 2019). Secondary formation is another important source
95 of atmospheric isocyanic acid and the known precursors include amides (Barnes et al.,
96 2010), urea (Jathar et al., 2017), and nicotine (Roberts et al., 2011; Borduas et al.,
97 2016). Amides are reported to be the main precursors of isocyanic acid in urban regions
98 (Wang et al., 2020). Isocyanic acid is the oxidative degradation product of amides

99 initiated by OH radicals, NO₃, radicals, and Cl atoms (*Barnes et al., 2010*). In addition
100 to primary emissions from organic solvents and various industrial processes, amides
101 can be also formed through the atmospheric accretion reactions of organic acids with
102 amines or ammonia (*Barnes et al., 2010; Yao et al., 2016*). Vertical gradient
103 measurements of HNCO can help elucidate potential formation sources and
104 mechanisms.

105 Chemical ionization mass spectrometry (CIMS) can effectively detect and
106 quantify atmospheric formic and isocyanic acids (*Bannan et al., 2014; Chandra and*
107 *Sinha, 2016; Liggio et al., 2017; Mungall et al., 2018; Fulgham et al., 2019*). CIMS
108 has been widely used onboard aircraft or on towers to make online vertical
109 measurements of formic and isocyanic acids (*Liggio et al., 2017; Mattila et al., 2018*).
110 Aircraft can carry many types of instruments and achieve measurements of a large suite
111 of parameters (*Benish et al., 2020; Zhao et al., 2021*), but the cost is also very expensive.
112 Towers can provide vertical observations of target species by setting up sites at different
113 heights, building mobile platforms (elevators or baskets) (*Mattila et al., 2018*), and
114 drawing air from multiple heights to the ground-based instruments through long tubes
115 (*Hu et al., 2013; Yáñez-Serrano et al., 2018*). The usage of long tubes is the most
116 convenient and cost-effective method to make gradient measurements of target gaseous
117 species so far. However, interactions between gaseous species and tubing walls may
118 bring unexpected uncertainties for their measurements (*Helmig et al., 2008a; Helmig*
119 *et al., 2008b; Schnitzhofer et al., 2009; Karion et al., 2010; Pagonis et al., 2017*).
120 Therefore, the impacts of long tubing on measurements of formic and isocyanic acids
121 need to be elucidated.

122 In this study, we first assessed the effects of long perfluoroalkoxy (PFA) Teflon
123 tubes on measurements of formic and isocyanic acids. Vertical gradient measurements
124 of the two acids were made through long tubes on a tall tower in urban Beijing, China.
125 Then, the vertical variations and sources of the two acids were investigated and
126 discussed. At last, key conclusions and implications of this study were summarized.

127 **2. Methods and materials**

128 **2.1. Site description and field campaign**

129 Vertical gradient measurements of gaseous species were made on the Beijing
130 Meteorological Tower, which is located on the campus of the Institute of Atmospheric
131 Physics (IAP), Chinese Academy of Sciences. Beijing is the capital city of China with
132 a population of over 20 million by 2020. Beijing has large anthropogenic emission
133 intensities and is suffering from severe air pollution problems (*Acton et al., 2020; Meng*
134 *et al., 2020; Tan et al., 2022*). The tower is located in the northern part of downtown
135 Beijing between the 3rd and 4th Ring Roads and is surrounded by urban roads,
136 expressways, residential areas, restaurants, urban landscaping, and parks. As a result,
137 concentrations of the primary pollutants at the tower site are mainly contributed by both
138 anthropogenic (e.g., vehicular exhausts, cooking, and household volatile chemical
139 products) and biogenic emissions. Detailed descriptions of the tower have been
140 provided in previous studies (*Acton et al., 2020; Yan et al., 2021*) and will not be
141 repeated here. The field campaign was carried out from July 17th to August 3rd, 2021.

142 **2.2. Instrumentation**

143 To obtain online gradient measurements of atmospheric trace gases, we
144 established a tower-based observation system using a combination of online
145 measurement techniques and long tubes (Figure S1). The system and related
146 assessments on the usage of long tubes have been explicitly described in our previous
147 study (*Li et al., 2023*) and will be briefly introduced here. After removing fine particles
148 by PFA Teflon filters (Whatman) with a diameter of 46.2 mm and a pore size of 2 μm ,
149 ambient air at four altitudes on the tower (namely 47, 102, 200, and 320 m) was
150 simultaneously and continuously drawn to the ground through long PFA Teflon tubes
151 (100, 150, 250, and 400 m; outer diameter: 1/2"; inner diameter: 0.374") by a vacuum
152 pump. [All the sampling tubes were installed inside the iron tower to avoid direct](#)
153 [sunlight.](#) The flow rate of the sample stream in each tube was controlled by a critical

154 orifice and ranged between 13-21 standard liters per minute (SLPM), as shown in table
155 S1. The flow rates in long tubes were retained as large as possible if instruments allowed
156 to minimize the impact of gas-surface interactions on measurements of targeted gaseous
157 species (*Deming et al., 2019; Li et al., 2023*). Two air-conditioned containers were
158 placed next to each other on the base of the tower and all the instruments were operated
159 inside. An additional inlet of the tube was mounted on the rooftop of the container
160 (approximately 5 m above ground level) to make measurements of trace gases near the
161 surface. Therefore, the tower-based observation system consisted of five inlet heights
162 ranging from the ground level to 320 m. Inlets of the instruments were connected to the
163 outlet of a Teflon solenoid valve group, which was used to perform the switch of the
164 inlet heights at time intervals of 4 minutes. Vertical gradient measurements of gaseous
165 species were cyclically made over periods of 20 minutes. Indoor PFA Teflon tubes were
166 wrapped with insulation tubes and were heated to prevent condensation of water and
167 organic gases.

168 Formic and isocyanic acids were measured by a high-resolution time-of-flight
169 chemical ionization mass spectrometry with iodide reagent ion (ToF-CIMS). Due to the
170 high sensitivity to oxygenated volatile organic compounds (OVOCs), the iodine ion
171 source has been widely used in previous studies (*Yuan et al., 2015; Schobesberger et*
172 *al., 2016; Mungall et al., 2018*). A Filter Inlet for Gases and AEROSols (FIGAERO)
173 was used to perform the switch between the gas and particle measurement modes
174 (*Lopez-Hilfiker et al., 2014*). The ion molecular reaction (IMR) chamber is adjacent to
175 the FIGAERO and utilizes a vacuum ultraviolet ion source (VUV-IS). Iodide anion (I^-)
176 is produced from the photoionization of methyl iodide (CH_3I) in IMR (*Ji et al., 2020*).
177 During the measurements, I^- was produced by introducing the CH_3I gas standard (1000
178 ppm, Dalian Special Gases, China) to the IMR chamber at a flow rate of 2 standard
179 cubic centimeters per minute (SCCM) in 200 SCCM high-purity nitrogen (N_2 ,
180 99.9995%) by the VUV-IS. The pressure of the IMR chamber was maintained at 70-80
181 mbar. Flow rates of the sample gas were maintained at 2 SLPM using a critical orifice.

182 During the field campaign, both gaseous and particle measurements were made through
183 the FIGAERO of the CIMS, but only gaseous measurements were analyzed in this study.
184 In a one-hour cycle, the first 24 min was allocated to make gaseous measurements
185 during which a complete vertical profile of a gaseous species can be obtained. [As shown](#)
186 [in Figure S3, there was no significant difference between the background signals of the](#)
187 [instrument made with and without the long tubes. Therefore, blank measurements of](#)
188 [the instrument were made by adding zero air just to the inlet of the instrument without](#)
189 [through the long tubes during the field campaign.](#) In the gaseous measurement mode, a
190 rapid blank measurement was made for 10 s at 3-min intervals in the first 21 min and a
191 long-time blank measurement was made in the rest 3 min (*Palm et al., 2019*). During
192 the first 21-min period of the one-hour cycle, another inlet at 5 m was used to collect
193 ambient particles using PTFE membrane filters (Zefluor®, Pall Inc., USA). Therefore,
194 the remaining 36 min of the one-hour cycle was allocated to analyze the collected
195 particle.

196 Calibrations of the ToF-CIMS for formic and isocyanic acids were performed in
197 the laboratory before and after the field campaign. Standard solutions of formic acid
198 were evaporated using the liquid calibration unit (LCU, IONICON Analytik GmbH)
199 and then diluted to designated concentration gradients by being mixed with zero air at
200 five flow rates. The gas standard of isocyanic acid is unstable at ambient temperature
201 and thus no commercial gas cylinder was available. Instead, cyanuric acid solution was
202 put into a diffusion cell and heated to 300 °C to generate isocyanic acid gas at a stable
203 mixing ratio. An ion chromatograph was used to quantify the concentration of the gas
204 standard by measuring deionized water that absorbed the isocyanic acid gas. Detailed
205 information about the isocyanic acid calibration procedure has been provided in our
206 previous work (*Wang et al., 2020*). Impacts of the changes in ambient humidity on
207 measurements of the ToF-CIMS for both formic and isocyanic acids were determined
208 in the laboratory and were corrected when calculating their respective concentrations.
209 Measured signals of the ToF-CIMS were processed using the Tofware software package

210 (version 3.0.3; ToFwerk AG, Switzerland).

211 A high-resolution proton-transfer-reaction quadrupole interface time-of-flight
212 mass spectrometry (PTR-ToF-MS) with both H_3O^+ and NO^+ ion chemistry was used to
213 measure reported precursors of the two acids, such as isoprene, aromatics, OVOCs, and
214 amides. Detailed information about the configuration and operation setup of the PTR-
215 ToF-MS has been provided in our previous studies (*Yuan et al., 2017; Wu et al., 2020;*
216 *Li et al., 2022*). Mixing ratios of O_3 , CO, and NO_2 were measured by a UV absorption
217 O_3 analyzer (T400, Teledyne API, USA), a gas filter correlation CO analyzer (T300,
218 Teledyne API, USA), and a trace level NO_x analyzer (42i, Thermo, USA), respectively.
219 Photolysis rates were measured by a PFS-100 photolysis spectrometer (Focused
220 Photonics Inc.) on the rooftop of the container. ~~The planetary boundary layer height~~
221 ~~(PBLH) data was obtained from the website of the Air Resources Laboratory~~
222 ~~(<https://ready.arl.noaa.gov/READYamet.php>).~~ The planetary boundary layer height
223 (PBLH) data was obtained from the web portal of the Real-time Environmental
224 Applications and Display sYstem (READY) of the National Oceanic and Atmospheric
225 Administration (NOAA) Air Resource Laboratory
226 (<https://ready.arl.noaa.gov/READYamet.php>). Measurements of isocyanic acid and
227 amides made in Guangzhou and Gucheng in China were also used in this study for
228 comparison, and more information about these observations can be found in our
229 previous papers (*Wang et al., 2020*).

230 **2.3. Tubing assessment**

231 The tower-based observation system used long PFA Teflon tubes (hundreds of
232 meters in length) to draw air samples from different heights. The interactions between
233 tubing inner walls and organic compounds, namely the absorption/desorption of trace
234 gases, have nonnegligible impacts on their measurements after traversing such long
235 tubes (*Pagonis et al., 2017; Deming et al., 2019*). The equilibrium between the
236 absorption and desorption of organic compounds on tubing walls required distinct times,
237 namely tubing delay, for different species. For nonpolar/weak-polar organic compounds,

238 their tubing delays and measurement uncertainties after traversing long tubes are
239 dependent on their saturation concentrations and the flow rates of sample streams but
240 are independent of changes in humidity (*Krechmer et al., 2017; Pagonis et al., 2017*).
241 For some small polar organic compounds, their tubing delays and measurement
242 uncertainties after traversing long tubes are dependent on Henry's law coefficients and
243 are affected by changes in humidity (*Liu et al., 2019*). The performance of long PFA
244 Teflon tubes in measuring concentrations of nonpolar/weak-polar organic compounds
245 and inorganic species (e.g., ozone, NO, NO₂, and CO₂) has been assessed in our
246 previous work (*Li et al., 2023*). The impacts of long PFA Teflon tubes on measurements
247 of formic and isocyanic acids are still unclear and will be assessed in this study.

248 Long PFA Teflon tubes with an outer diameter of 1/2" and an inner diameter of
249 0.374" were used to draw air samples from different altitudes and thus were assessed.
250 At flow rates below 20 SLPM, suitable pressure drops can be maintained in these long
251 tubes for instrument operation (*Li et al., 2023*). The effects of long tubes on
252 measurements of formic and isocyanic acids were mainly assessed using the same
253 methods in the literature (*Li et al., 2023*). The tubing delay of formic acid is estimated
254 as the time required to reach 90% of the concentration change made at the tubing inlet.
255 ~~The depassivation curve of formic acid measured at the air outlet end of the tubing was~~
256 ~~used to calculate its tubing delay and was obtained by using a step-function change in~~
257 ~~its concentration at the tubing inlet~~ The depassivation curve of formic acid measured at
258 the outlet end of the long tubing was used to calculate its tubing delay and was obtained
259 by using a step-function change of the formic acid concentration from 7.5 ppbv to 0
260 ppbv at the tubing inlet (*Pagonis et al., 2017; Deming et al., 2019*). The formic acid
261 signals were normalized to those measured at the beginning of the step-function change
262 and then were fitted using the double exponential method, as shown in Figure 1. Finally,
263 the tubing delay of formic acid was determined when the fitting line decreased to 0.1.
264 The previous study (*Li et al., 2023*) has reported that inorganic species have small
265 tubing delays even in a 400 m long tube. Therefore, tubing delays of isocyanic acid in

266 long tubes are not discussed in this study.

267 To further assess the impacts of long tubes (namely 100, 200, 300, and 400 m)
268 on measurements of formic and isocyanic acids in real environments, their ambient
269 mixing ratios measured through different lengths of tubes were intercompared by
270 running the inlets side by side at ground level. Ambient air samples were sequentially
271 drawn with and without the tubes through a Teflon solenoid valve group (Figure S2),
272 which was set to perform the switch at time intervals of 4 minutes. Instrument
273 backgrounds of the two species were measured for 10 s at time intervals of 1 minute by
274 passing zero air into the instrument at a flow rate of 3 SLPM. Inter-comparisons of the
275 formic acid and isocyanic acid measurements made through different lengths of tubes
276 were mainly performed using linear fittings ($y=kx+b$; k is the slope and b is the
277 intercept).

278 **3. Results and Discussions**

279 **3.1. Interactions between long tubes and the two acids**

280 As shown in Figure 1, signals of formic acid measured by the ToF-CIMS had a
281 tubing delay of 23 s after traversing the 400 m long tube at the flow rate of 13 SLPM.
282 In addition to the interactions between tubing walls and formic acid molecules (*Pagonis*
283 *et al.*, 2017; *Deming et al.*, 2019), molecular diffusion and dispersion (namely Taylor
284 dispersion) can cause the longitudinal mixing of gas molecules in the tubing and is also
285 an important factor contributing to the measured delays (*Karion et al.*, 2010). Molecular
286 diffusion and dispersion have strong dependences on molecular diffusion coefficients
287 and tubing flow rates (*Karion et al.*, 2010). The influential time of Taylor dispersion on
288 the measurements of formic acid through a 400 m long tube at the flow rate of 13 SLPM
289 was estimated to be only 2.9 s, which is much smaller than the measured tubing delay
290 (23 s) of formic acid. Therefore, the adsorption/desorption of formic acid molecules on
291 tubing inner walls plays a dominant role in determining the tubing delay.

292 For most organic compounds, the tubing delays generally depend on tubing flow

293 rates and their saturated concentrations (C^*) (Li et al., 2023; Deming et al., 2019). With
294 the increase in tubing length and flow rate, the tubing delays of organic compounds will
295 rapidly decrease (Liu et al., 2019). Therefore, the tubing flow rates should be as large
296 as possible if the instrument could work normally. In addition, the tubing delays of
297 organic compounds generally increase with the decrease in their C^* (Li et al., 2023). It
298 must be acknowledged that tubing delay is inevitable. The analysis time scales of
299 species concentrations measured through long tubes should be greater than their tubing
300 delays, especially for those with small C^* .

301 The delay time of formic acid mentioned here is different from the residence time
302 of the gas through the long tubing. Residence time refers to the time required for the
303 sample gas to pass through the tubes. As for the measured tubing delays of trace gases,
304 they refer to the amounts of time required for the instruments to measure stable
305 concentrations of targeted species in response to a change in species concentrations at
306 the tubing inlet. The residence time is the same for all trace gases, depending on the
307 length of the long tube, the inner diameter of the tube, and the flow rate of the sample
308 gas. However, the tubing delay for each trace gas is different and depends on the flow
309 rate, their respective saturated concentrations/Henry's constants, and molecular
310 diffusion and diffusion rates. The difference between residence time and delay time is
311 also discussed in detail in our previous work (Li et al., 2023).

312 As shown in Figure S3S4(a), ambient mixing ratios of formic acid measured
313 through the 400 m long tube varied consistently with those measured without the tube
314 with mean values of 4.14 and 4.09 ppbv, respectively. The mixing ratios of formic acid
315 measured with the long tube were slightly higher in the daytime and lower at night in
316 comparison with those measured without the long tube. We also conducted a correlation
317 analysis between the mixing ratios of formic acid measured with and without long tubes.
318 As shown in Figure 2, the mixing ratios of formic acid measured with and without the
319 400 m long tube agreed within 20%, but the slope of the linear fitting ($k=0.84$) is lower
320 than 1. The differences of formic acid mixing ratios measured with and without the 400

321 m long tube were predominantly caused by the long-tail memory effect of the tubing
 322 (Figure 1). For example, the mixing ratios of formic acid measured through the 400 m
 323 long tube at night equaled to its ambient mixing ratios plus those released from the
 324 tubing inner wall. The tubing delay of formic acid was determined when its mixing
 325 ratios reached 90% of the change before entering the tubing. However, the long-tail
 326 memory effect of the tubing mainly focused on the rest 10% of the change (Figure 1),
 327 which required a much longer time to stabilize.

328 Impacts of the tubing memory effects will be accumulated due to the continuous
 329 change in ambient concentrations of formic acid. To further assess the impacts of tubing
 330 memory effects on measurement uncertainties of the two acids, differences between
 331 mixing ratios of the species X (namely formic and isocyanic acids) measured with and
 332 without long tubes at time t (denoted by $\delta[X]_t$) were calculated using Eq. (1):

$$333 \quad \delta[X]_t = [X_{without}]_t - [X_{with}]_t \quad (1)$$

334 where $[X_{with}]_t$ and $[X_{without}]_t$ refer to mixing ratios of the species X measured at
 335 time t with and without long tubes, respectively; ~~Δt is the change in time relative to~~
 336 ~~time t and was used to characterize the influential time of the memory effect.~~ In addition,
 337 the changes in mixing ratios of the species X measured using long tubes was also
 338 calculated using Eq. (2): ~~at time t relative to its average mixing ratio over the previous~~
 339 ~~time interval of Δt (denoted by $\Delta[X]_t$) was also calculated using Eq. (2):~~

$$340 \quad \Delta[X]_t = [X_{with}]_t - \frac{\sum_{t-\Delta t}^t [X_{with}]}{\Delta t} \quad (2)$$

341 where Δt is the change in time relative to time t and was used to characterize the
 342 influential time of the memory effect. A strong correlation between $\delta[X]_t$ and $\Delta[X]_t$
 343 could be captured at a certain Δt if the tubing memory effect make essential
 344 contributions to measurement uncertainties of the species X after traversing long tubes.
 345 For the 400 m long tubing, $\delta[X]_t$ and $\Delta[X]_t$ had the strongest correlation ($R^2=0.89$)
 346 when Δt was approximately 14 h (Figure S5S7). As also shown in Figure 2(a), the
 347 mixing ratios of formic acid measured with and without the 400 m long tube agreed
 348 well when $\Delta[HCOOH]$ approached to zero. The decrease and increase in $\Delta[HCOOH]$

349 will enlarge measurement uncertainties of formic acid using the long tube. In morning
350 periods, ambient mixing ratios of formic acid rapidly increased. As a result, the mixing
351 ratios of formic acid measured through the 400 m long tube were slightly lower than its
352 ambient mixing ratios due to the absorption of formic acid by tubing inner walls. In
353 evening and nighttime periods, an opposite phenomenon was observed due to the
354 desorption of formic acid from tubing inner walls (Figure S3S4).-

355 In addition to the 400 m long tube, impacts of the tubes with lengths of 100, 200,
356 and 300 m on measurements of formic acid were also assessed, as shown in Figures 2(c)
357 and 3(a). The usage of tubes with lengths of 100, 200, and 300 m has negligible impacts
358 on the measurements of formic acid. During the test of the 200 m tubing, meteorological
359 conditions significantly changed with lower temperatures and stronger winds in
360 comparison to the days on which the tests of the other lengths of tubes were performed.
361 As shown in Figure S5, the concentrations of formic acid and isocyanic acid were
362 evidently enhanced and significantly varied during the 400 m tubing test. In contrast,
363 ambient concentrations of formic and isocyanic acid were relatively low and slightly
364 varied, resulting in the exceedingly large or low values of k and R^2 between the
365 concentrations of formic acid measured with and without the 200 m long tubing.
366 However, according to the results of the test, the average concentration difference of
367 formic and isocyanic acid measured with and without the 200 m tubing agreed well
368 within 4%, suggesting that the 200 m long tube has minor effects on the measurements
369 of formic and isocyanic acid.

370 In contrast to formic acid, the usage of long tubes had minor impacts on the
371 measurements of isocyanic acid. The mixing ratios of isocyanic acid measured with and
372 without the 400 m long tube varied consistently ($k=0.86$, $R^2=0.90$) with mean values of
373 0.25 and 0.26 ppbv, respectively (Figure S3S4). As shown in Figure 2(b), $\Delta[HNCO]$
374 is evenly distributed on both sides of the 1:1 line. Therefore, the changes in ambient
375 concentrations of isocyanic acid do not have significant impacts on the measurements
376 of isocyanic acid through the long tubes. As also shown in Figure 3(b), $\delta[HNCO]$ and

377 $\Delta[HNCO]$ of isocyanic acid were independent of the changes in isocyanic acid mixing
378 ratios. The R^2 values of linear fittings were less than 0.21 for the isocyanic acid
379 measurements made using different lengths of tubes. This is consistent with the results
380 reported in the literature (*Helmig et al., 2008a; Helmig et al., 2008b; Li et al., 2023*)
381 that inorganic species with low reactivities can be well measured using long PFA Teflon
382 tubes. ~~The test results confirm that the measurements of formic and isocyanic acids~~
383 ~~made through long tubes can be used to characterize their vertical and temporal~~
384 ~~variations.~~ The test results confirmed that the measurements of formic acid and
385 isocyanic acid through long tubes can be used to characterize their vertical and temporal
386 variability. However, a further correction of the formic acid measurements made
387 through the long tubes must be performed if they were used to accurately calculate the
388 kinetic parameters of chemical reactions regarding the formation and removal of formic
389 acid at different heights.

390 **3.2. Vertical variations and sources of formic acid**

391 Time series of formic acid and ozone mixing ratios at 5 and 320 m are shown in
392 Figure 4. The concentrations of formic acid and ozone exhibited similar diurnal and
393 inter-diurnal variations at different altitudes during the campaign. Hourly mean mixing
394 ratios of ozone exhibited strong temporal variations with an average of 43.5 ± 25.3 ppbv
395 at 5 m and an average of 53.5 ± 25.0 ppbv at 320 m. Hourly mean mixing ratios of formic
396 acid at 5 m ranged between 0.1–6.6 ppbv with an average of 1.3 ± 1.3 ppbv at 5 m, which
397 is comparable to those observed in other megacities, such as Shenzhen (1.2 ppbv) in
398 China (*Zhu et al., 2019*), London (1.3 ppbv) in UK (*Bannan et al., 2017*), and Los
399 Angeles (2.0 ppbv) in USA (*Yuan et al., 2015*). By contrast, hourly mean mixing ratios
400 of formic acid at 320 m had an average of 2.1 ± 1.9 ppbv, approximately 1.6 times higher
401 than that at 5 m. The temporal variability of formic and isocyanic acids were mainly
402 caused by the diurnal and inter-diurnal changes in meteorological conditions (e.g., solar
403 radiation and PBLH).

404 Before July 12th, the daily maximum hourly mixing ratios of ozone at 5 m all

405 exceeded 100 ppbv, indicating the enhanced formation of secondary air pollutants
406 associated with photochemical reactions. The mixing ratios of formic acid measured
407 before July 12th were also prominently larger than those measured after, suggesting
408 important contributions from photochemical formations. The photochemical formation
409 of secondary pollutants was weak from July 13th to 30th due to the cloudy and rainy
410 weather. After August 1st, low mixing ratios of ozone and formic acids were observed
411 along with the occurrence of favorable dilution conditions characterized by high PBLHs.

412 As shown in Figure 5, the mixing ratios of formic acid measured at the five
413 altitudes (namely 5, 47, 102, 200, and 320 m) exhibited similar diurnal patterns. After
414 sunrise (~6:00 LT), formic acid mixing ratios increased rapidly at each altitude before
415 reaching the peak between 14:00-16:00 LT and then continuously declined before
416 sunrise the following day. Similar diurnal variation patterns of formic acid were also
417 observed at other urban sites (*Veres et al., 2011*), rural sites (*Hu et al., 2022*), and remote
418 sites (*Schobesberger et al., 2016*). The diurnal variation patterns of formic acid were
419 highly similar to those of ozone (a typical secondary pollutant) but were different from
420 those of VOCs from primary emissions. Taking toluene as an example, toluene is a
421 typical VOC tracer of anthropogenic emission sources in urban regions, such as
422 industrial processes and vehicular exhausts (*Fang et al., 2016; Skorokhod et al., 2017*),
423 and is also an important precursor of ozone (*Yuan et al., 2012*). The mixing ratios of
424 toluene exhibited opposite diurnal variation patterns to those of ozone and formic acids
425 with the minima occurring at around 14:00 LT. The lower mixing ratios of toluene in
426 daytime than in nighttime were predominantly caused by the enhancement of
427 atmospheric dilution and chemical removal by OH radicals (*De Gouw et al., 2018*). The
428 mixing ratios of formic acid poorly correlated (R^2 ranged between 0.16-0.28) with those
429 of CO (a typical tracer of combustion sources) at the five altitudes but well correlated
430 (R^2 ranged between 0.67-0.75) with those of Ox (O_3+NO_2 , a conserved metric of ozone
431 by removing NO titration effect), as shown in Figure 6. These results further confirm
432 that ambient concentrations of formic acid in urban Beijing were dominantly

433 contributed by secondary sources associated with photochemical reactions rather than
434 primary emissions.

435 Another observed evidence for the dominant contribution of formic acid from
436 secondary formations is its positive vertical gradients in nighttime (defined as the
437 period of 22:00-5:00 LT), as shown in Figure 7. Large amounts of formic acid will
438 accumulate near the surface with strong negative vertical gradients if primary emissions
439 dominate its contributions, as manifested by vertical toluene profiles. At nighttime, the
440 mixing ratios of ozone also increased with height due to enhanced removal by NO
441 titration and surface dry deposition. The deposition of formic acid was also enhanced
442 near the surface, driving the formation of positive gradients in vertical formic acid
443 profiles.

444 A notable difference existed between the diurnal variation patterns of ozone and
445 formic acid above the ground. As shown in Figure 5, the mean mixing ratios of ozone
446 at 5 m rapidly increased from 21.5 ppbv to 36.0 ppbv from 6:00 to 10:00 LT, while the
447 mean mixing ratios of ozone at 320 m slightly increased from 16.3 ppbv to 16.9 ppbv
448 during the same period. The enhancement rate is defined as the average change rate of
449 the species concentration between two adjacent hours. As shown in Figure 8, the
450 enhancement rates of ozone mixing ratios between 6:00 and 10:00 LT decreased with
451 the increase in height. This phenomenon indicates relatively weak photochemical ozone
452 formation in urban regions aloft before 10:00 LT due to the lack of reactive ozone
453 precursors (e.g., unsaturated hydrocarbons and NO_x). With the enhancement of the
454 vertical exchange of air masses with the rise of the boundary layer, large amounts of
455 ozone precursors (e.g., the observed peaks of toluene mixing ratios at 320 m at 10:00
456 LT) emitted from surface sources were transported upward and drove the formation of
457 ozone in high altitudes. In contrast to ozone, the mixing ratios of formic acid at the five
458 altitudes all increased rapidly between 6:00 and 10:00 LT. The enhancement rate of
459 formic acid mixing ratios between 6:00 and 10:00 LT kept nearly constant below 320
460 m (Figure 8). This result implies that the oxidation products of VOCs over nighttime or

461 in the daytime before are important precursors of formic acid and can drive the rapid
462 formation of formic acid with further photooxidation. This speculation can be supported
463 by the vertical and diurnal variations of methyl vinyl ketone (MVK), methacrolein
464 (MACR), and formaldehyde, which are reported key precursors of formic acid as shown
465 in Figure 5(d) and 5(e). The diurnal variation patterns of MVK+MACR and
466 formaldehyde at the five latitudes were nearly the same with the enhancements in
467 daytime. In addition, concentrations of MVK+MACR and formaldehyde all increased
468 with height in nighttime and early morning periods, facilitating the photochemical
469 formation of formic acid even in the residual layer.

470 As a reactive hydrocarbon species, the mixing ratios of toluene rapidly decreased
471 with height in daytime (defined as the period of 11:00-16:00 LT, as shown in Figure 7)
472 due to the combined effects of atmospheric dilution and OH-initiated chemical removal.
473 By contrast, the mixing ratios of ozone and formic acid increased with height. The
474 mixing ratios of ozone and formic acid all rapidly increased with height below 102 m,
475 predominantly attributed to the reduced effect of surface dry deposition with the
476 increase in height. The mean mixing ratios of formic acid increased by 18% from 102
477 m to 320 m in daytime, while ozone mixing ratios were well mixed above 102 m. Our
478 results point to the likely importance of photochemistry as a source of formic acid that
479 is enhanced with increasing height within the boundary layer.

480 The precursors and formation mechanisms of atmospheric formic acid have been
481 extensively investigated in previous studies but still remain uncertain. Isoprene has long
482 been recognized as an important precursor of formic acid through reactions with O₃ and
483 OH radicals (*Neeb et al., 1997; Paulot et al., 2009*). Recent studies also found that the
484 degradation of organic aerosols (OA) derived from isoprene is an important source of
485 formic acid (*Cope et al., 2021; Bates et al., 2023*). In addition, the photooxidation of
486 other biogenic and anthropogenic hydrocarbons is also a key source of formic acid
487 (*Paulot et al., 2011; Millet et al., 2015; Link et al., 2021*). Figure 9 illustrates the mean
488 vertical profiles of several key precursors of formic acid in daytime. The concentrations

489 of isoprene and toluene (Figure 7) all decreased rapidly with height. By contrast, MVK
490 and MACR, the primary oxidation products of isoprene (*Grosjean et al., 1993*),
491 exhibited weak vertical gradients. Formaldehyde, a more general photooxidation
492 product of VOCs, exhibited similar vertical distribution patterns to those of ozone.
493 Large amounts of OVOCs were produced and accumulated in higher altitudes through
494 the oxidation of hydrocarbons and the further oxidation of some OVOCs during their
495 upward mixing course. MVK, MACR, and formaldehyde are also key precursors of
496 formic acid. MVK and MACR can react with O₃ to produce formic acid (*Link et al.,*
497 *2020*). Formaldehyde can be converted to methanediol in cloud droplets and then be
498 rapidly oxidized by OH to produce formic acid (*Franco et al., 2021*). In addition, enol
499 (*Lei et al., 2020*) and many other OVOCs (such as glycolaldehyde (*Butkovskaya et al.,*
500 *2006a*) and hydroxyacetone (*Butkovskaya et al., 2006b*) can be further oxidized to
501 produce formic acid. Therefore, high concentrations of OVOCs aloft may be the
502 dominant factor that largely enhances the photochemical formation of formic acid in
503 urban regions.

504 As discussed above, formic acid exhibited strong positive vertical gradients
505 throughout the day, implying that the concentrations of formic acid measured at ground
506 level were not capable of accurately characterizing its abundance and temporal
507 variability in the whole boundary layer. Besides, the formic acid formed in daytime and
508 retained in the nocturnal residual layer also has vital impacts on the budget of formic
509 acid in the boundary layer. Thus, we used the column-integrated concentration (CIC)
510 of formic acid (the sum of the abundance in both the nocturnal residual layer and the
511 boundary layer, see detailed definitions in SI) to further clarify the diurnal variability
512 in the abundance of formic acid in the boundary layer.

513 As shown in Figure 10, the CICs of formic acid had a flatter diurnal pattern in
514 comparison to those at ground level. The CICs of formic acid had approximately stable
515 values overnight and reached a maximum at 16:00 LT. The ratio of the maximum and
516 minimum of CIC for formic acid was only 1.3, while it was 4.2 for the concentrations

517 of formic acid at 5 m. The ground-level measurements were more affected by
518 depositional losses, while such depositional losses in the residual layer were nearly
519 absent. However, the chemical species retained in the residual layer were closely related
520 to their budgets in the daytime boundary layer. If the removal rates of formic acid from
521 ground-level measurements were used to characterize those at high altitudes (e.g., in
522 the residual layer), the removal of formic acid in the entire boundary layer would be
523 ~~overestimated. These results imply that the removal of atmospheric formic acid (e.g.,~~
524 ~~surface deposition and various chemical reactions) may be highly overestimated if only~~
525 ~~ground level measurements were used or constrained in numerical models. The budget~~
526 ~~of the formic acid in high altitudes in the boundary layer was distinctly different from~~
527 ~~those near the surface.~~ As the result, numerical models cannot accurately reproduce the
528 abundances and budgets of formic acid without the constraints of vertical observations
529 and the clarification of formic acid formation mechanisms.

530 **3.3. Vertical variations and sources of isocyanic acid**

531 The mixing ratios of isocyanic acid also exhibited strong temporal variations
532 during the campaign with a mean of 0.28 ± 0.16 ppbv at 5 m and a mean of 0.43 ± 0.21
533 ppbv at 320 m, as shown in Figure 11. The mixing ratios of isocyanic acid measured at
534 the ground level in urban Beijing were approximately 10 times higher than those
535 measured in Los Angeles, USA (0.025 ppbv) (Roberts *et al.*, 2014) and Calgary, Canada
536 (0.036 ppbv) (Woodward-Massey *et al.*, 2014) but were lower than those measured in
537 other regions in China. For example, the mean mixing ratio of isocyanic acid was 0.37
538 ppbv at a rural site (Gucheng) in the North China Plain (NCP), and 0.46 ppbv in urban
539 Guangzhou in the Pearl River Delta (PRD) region (Wang *et al.*, 2020). Isocyanic acid
540 will pose a threat to human health when its ambient mixing ratios exceed 1.0 ppbv. In
541 this study, isocyanic acid mixing ratios greater than 1.0 ppbv were not observed at
542 ground level but were observed at 320 m on three days. The maximum hourly mixing
543 ratios of isocyanic acid at 320 m reached 1.63 ppbv at 16:00 LT on July 8th.

544 The mixing ratios of isocyanic acid at the five altitudes exhibited similar diurnal

545 variation patterns. After sunrise, the mixing ratios of isocyanic acid at the five altitudes
546 all simultaneously increased and peaked at about 14:00 LT. Then, isocyanic acid mixing
547 ratios decreased slowly and reached the minimum before sunrise the following day.
548 This diurnal variation pattern of isocyanic acid measured at the ground level in urban
549 Beijing was not consistent with those measured at the Gucheng site in NCP (*Wang et*
550 *al.*, 2020). The isocyanic acid mixing ratios at the Gucheng site exhibited insignificant
551 diurnal variability throughout the day with only a weak morning peak, predominantly
552 attributed to the enhancement of primary emissions. However, the diurnal variation
553 patterns of isocyanic acid measured at the five altitudes were well correlated with the
554 change in solar irradiance and were consistent with those measured at the two sites in
555 PRD. These results imply that ambient concentrations of isocyanic acid in urban Beijing
556 were mainly contributed by secondary sources associated with photochemical reactions.

557 Similar to formic acid, the simultaneous increase of isocyanic acid mixing ratios
558 at the five altitudes with the onset of sunlight also indicates the presence of adequate
559 precursors even in the nocturnal residual layer. In addition, the diurnal variability of
560 isocyanic acid mixing ratios measured below 200 m was much weaker than those
561 measured at 320 m. For example, the ratio of the daily maximum to the daily minimum
562 mixing ratios of isocyanic acid was 1.9 at 320 m, while the ratio was only 1.4 at 5 m.
563 The mean enhancement rate of isocyanic acid mixing ratios at 320 m (0.05 ppbv h^{-1})
564 between 6:00 and 10:00 LT was approximately five times larger than that at 5 m (0.01
565 ppbv h^{-1}). The vertical gradients of isocyanic acid between 102 and 320 m were also
566 larger than those below (Figure 12). The rapid increase in both concentrations and
567 enhancement rates of isocyanic acid with height (Figures 8 and 12) implies the
568 enhanced photochemical formation of isocyanic acid in the middle and upper part of
569 the boundary layer.

570 Secondary formation precursors of atmospheric isocyanic acid were still poorly
571 understood so far. Amides were considered important precursors of isocyanic acid
572 (*Roberts et al.*, 2014; *Rosanka et al.*, 2020). As reported in our previous study (*Wang*

573 *et al.*, 2020), C₃ amides accounted for the largest fraction of the total concentrations of
574 amides and were dominant contributors to the secondary formation of isocyanic acid.
575 The mixing ratios of C₃ amides in Guangzhou in PRD exhibited strong diurnal
576 variations. Along with the sunrise, the mixing ratios of C₃ amides rapidly decreased and
577 reached the minimum at 13:00 LT. Afterward, the mixing ratios of C₃ amides started to
578 increase and accumulated at night. As shown in Figure S4S6, the influence of long
579 tubing on the measurement of amides was limited, so we also measured the amides
580 during the field campaign. However, the mixing ratios of C₃ amides in Beijing and
581 Gucheng in NCP exhibited insignificant diurnal variability, consistent with those of
582 isocyanic acid. The mean mixing ratios of C₃ amides at 5 m in urban Beijing is only
583 0.03 ppbv during the campaign, which is one order of magnitude lower than those in
584 Guangzhou (0.35 ppbv) and Gucheng (0.18 ppbv). The mixing ratios of C₃ amides
585 measured at the five altitudes in urban Beijing were also approximately one order of
586 magnitude lower than those of isocyanic acid (Figure 12). Besides, the mixing ratios of
587 C₃ amides decreased with height in both nighttime and daytime, indicating predominant
588 contributions from primary emissions. This is consistent with the fact that primary
589 emissions of chemical composition from industry-related sources have been largely
590 reduced with the outward migration of industry in urban Beijing. By contrast, the
591 mixing ratios of isocyanic acid increased with height in both day and night with an
592 average of 0.32 ppbv at 5 m and 0.60 ppbv at 320 m. These results suggest that C₃
593 amides were far more enough to account for the secondary formation of isocyanic acid
594 in urban Beijing.

595 Figure 13(a) gives the composition and average concentrations of C₁-C₁₀ amides
596 measured at the five altitudes during the campaign. C₂ amides accounted for the largest
597 fraction of the total mixing ratios of amides. The total mixing ratios of amides exhibited
598 decreasing tendencies with the increase in height, suggesting predominant contributions
599 from direct emissions of surface sources. As for formamide, its mixing ratios exhibited
600 an increasing tendency from 0.024 ppbv at 5 m to 0.030 ppbv at 320 m. The positive

601 vertical gradients of formamide suggest its enhanced formation with height, probably
602 due to the enhancements of formic acid. However, the average concentration ratios of
603 formamide to formic acid slightly varied between 0.01 and 0.02 among the five heights.
604 The average concentration ratios of formamide to isocyanic acid decreased from 0.09
605 at 5 m to 0.07 at 320 m. These results imply that the formation of isocyanic acid through
606 the pathway of $\text{HCOOH-CH}_3\text{NO-HNCO}$ may be enhanced with the increase in height
607 but could only contribute a tiny fraction of the observed isocyanic acid, as shown in
608 Figure 13(b). Assuming the full conversion of $\text{C}_1\text{-C}_{10}$ amides to isocyanic acid, the
609 average concentration ratios of amides (sum of $\text{C}_1\text{-C}_{10}$) to isocyanic acid below 320 m
610 only ranged between 0.32 and 0.56 and decreased with height. Therefore, in addition to
611 amides, there must be other important precursors and formation pathways of isocyanic
612 acid, particularly in high altitudes. The simultaneous increase of isocyanic acid
613 concentrations at the five heights upon sunrise (Figure 11) implies the presence of
614 adequate precursors in the nocturnal residual layer. The oxidation products of VOCs
615 driven by ozone and NO_3 radicals in nighttime may be an important class of precursors.
616 In addition, the largest enhancement rates and highest concentrations of isocyanic acid
617 at 320 m in daytime also suggest that high concentrations of OVOCs and low- NO_x
618 conditions may enhance the secondary formation of isocyanic acid.

619 The positive vertical gradients of isocyanic acid imply that the secondary
620 formation of isocyanic acid aloft could serve as an important source of surface isocyanic
621 acid in daytime driven by turbulence mixing. The CICs of isocyanic acid were
622 calculated to further clarify its abundance and temporal variability in the whole
623 boundary layer. Distinct diurnal patterns were observed between the ground-level
624 concentrations and CICs of isocyanic acid. Analogous to formic acid, the CICs of
625 isocyanic acid varied insignificantly over nighttime and enhanced in daytime, reaching
626 the maximum at approximately 14:00 LT. The formation of some chemicals can be
627 largely enhanced at higher altitudes and so using ground-level measurements to
628 constrain numerical models may be not adequate.

629 **4. Conclusion**

630 In this study, vertical and diurnal variations of formic and isocyanic acids in
631 urban Beijing were investigated using tower-based online gradient measurements. The
632 measurements of isocyanic acid can be well measured through long PFA Teflon tubes.
633 The measurements of formic acid made through long tubes were slightly influenced by
634 the memory effect of tubing walls, and the vertical increasing gradients of formic acid
635 may be slightly enhanced if the tubing effects were considered. The concentrations of
636 formic and isocyanic acids all increased with height in both nighttime and daytime. The
637 diurnal and vertical distribution patterns of formic and isocyanic acids all suggest that
638 their abundances in the boundary layer were dominantly contributed by secondary
639 formation associated with photochemical reactions. The photochemical formations of
640 formic and isocyanic acids were also substantially enhanced with the increase in height.
641 The formation pathway of isocyanic acid through $\text{HCOOH-CH}_3\text{NO-HNCO}$ only
642 accounted for a tiny fraction of its ambient abundance. The formic and isocyanic acids
643 photochemically formed in the middle and upper parts of the boundary layer were
644 important sources for those at ground level in urban region. The differences of the
645 diurnal patterns between CICs and ground-level concentrations of formic and isocyanic
646 acids further highlight the importance of vertical observations in elucidating their
647 budgets and sources in the whole boundary layer.

648 Characterization of the vertical variations in formic and isocyanic acids could
649 provide valuable information for elucidating their budgets and sources in the boundary
650 layer. However, there are still many important but unresolved questions associated with
651 the vertical distributions of formic and isocyanic acids. For example, the key precursors
652 that drive the rapid formation of formic and isocyanic acids in the residual layer are still
653 unknown. Are there any changes in the key precursors and formation pathways of
654 formic and isocyanic acids with the increase of height in urban region? To answer these
655 questions, the combination of vertical gradient measurements of more chemical species
656 and numerical simulations is needed in future studies.

657 **Supporting Information:** Additional experimental details, materials, and methods,
658 including schematic illustration of tubing test, determination of the long tubes'
659 cumulative influence, and calculation of CICs.

660 **Data availability**

661 Data related to this article are available online at
662 <https://doi.org/10.7910/DVN/ANH0WE>.

663 **Author contributions**

664 QY, XBL, BY, and YH designed the research. QY, XBL, BY, XZ, YH, LY, XH,
665 JQ and MS contributed to the data collection and data analysis. QY and XBL wrote the
666 paper with contributions from all coauthors. All the coauthors discussed the results and
667 reviewed the paper.

668 **Competing interests**

669 The authors declare that they have no conflict of interest.

670 **Acknowledgment**

671 This work was financially supported by the National Key R&D Plan of China
672 (grant No. 2023YFC3706103, 2023YFC3706201, 2022YFC3700604) and the National
673 Natural Science Foundation of China (grant No. 42121004, 42275103,
674 [42205904](#)[42205094](#), 42230701, 42305095). This work was also supported by the
675 Special Fund Project for Science and Technology Innovation Strategy of Guangdong
676 Province (Grant No. 2019B121205004). The authors would like to thank the personnel
677 who participated in data collection, instrument maintenance, and logistic support during
678 the field campaign.

679 **Reference**

680 Acton, W. J. F., Huang, Z., Davison, B., Drysdale, W. S., Fu, P., Hollaway, M., Langford,
681 B., Lee, J., Liu, Y., Metzger, S., Mullinger, N., Nemitz, E., Reeves, C. E., Squires, F.
682 A., Vaughan, A. R., Wang, X., Wang, Z., Wild, O., Zhang, Q., Zhang, Y., and Hewitt,

683 C. N.: Surface–atmosphere fluxes of volatile organic compounds in Beijing,
684 Atmospheric Chemistry and Physics, 20, 15101-15125, 10.5194/acp-20-15101-2020,
685 2020.

686 Alwe, H. D., Millet, D. B., Chen, X., Raff, J. D., Payne, Z. C., and Fledderman, K.:
687 Oxidation of Volatile Organic Compounds as the Major Source of Formic Acid in a
688 Mixed Forest Canopy, Geophysical Research Letters, 46, 2940-2948,
689 <https://doi.org/10.1029/2018GL081526>, 2019.

690 Andreae, M. O., Talbot, R. W., Andreae, T. W., and Harriss, R. C.: Formic and acetic
691 acid over the central Amazon region, Brazil: 1. Dry season, Journal of Geophysical
692 Research: Atmospheres, 93, 1616-1624, <https://doi.org/10.1029/JD093iD02p01616>,
693 1988.

694 Bannan, T. J., Bacak, A., Muller, J. B. A., Booth, A. M., Jones, B., Le Breton, M.,
695 Leather, K. E., Ghalaieny, M., Xiao, P., Shallcross, D. E., and Percival, C. J.:
696 Importance of direct anthropogenic emissions of formic acid measured by a chemical
697 ionisation mass spectrometer (CIMS) during the Winter ClearfLo Campaign in
698 London, January 2012, Atmospheric Environment, 83, 301-310,
699 10.1016/j.atmosenv.2013.10.029, 2014.

700 Bannan, T. J., Murray Booth, A., Le Breton, M., Bacak, A., Muller, J. B. A., Leather, K.
701 E., Khan, M. A. H., Lee, J. D., Dunmore, R. E., Hopkins, J. R., Fleming, Z. L., Sheps,
702 L., Taatjes, C. A., Shallcross, D. E., and Percival, C. J.: Seasonality of Formic Acid
703 (HCOOH) in London during the ClearfLo Campaign, Journal of Geophysical
704 Research: Atmospheres, 122, 10.1002/2017jd027064, 2017.

705 Barnes, I., Solignac, G., Mellouki, A., and Becker, K. H.: Aspects of the atmospheric
706 chemistry of amides, ChemPhyChem, 11, 3844-3857, 10.1002/cphc.201000374,
707 2010.

708 Bates, K. H., Jacob, D. J., Cope, J. D., Chen, X., Millet, D. B., and Nguyen, T. B.:
709 Emerging investigator series: aqueous oxidation of isoprene-derived organic aerosol
710 species as a source of atmospheric formic and acetic acids, Environmental Science:
711 Atmospheres, 10.1039/d3ea00076a, 2023.

712 Benish, S. E., He, H., Ren, X., Roberts, S. J., Salawitch, R. J., Li, Z., Wang, F., Wang,
713 Y., Zhang, F., Shao, M., Lu, S., and Dickerson, R. R.: Measurement report: Aircraft
714 observations of ozone, nitrogen oxides, and volatile organic compounds over Hebei
715 Province, China, Atmospheric Chemistry and Physics, 20, 14523-14545,
716 10.5194/acp-20-14523-2020, 2020.

717 Borduas, N., Murphy, J. G., Wang, C., Silva, G. d., Abbatt, J. P. D. J. E. S., and Letters,
718 T.: Gas Phase Oxidation of Nicotine by OH Radicals: Kinetics, Mechanisms, and
719 Formation of HNCO, 3, 327-331, 2016.

720 Butkovskaya, N. I., Pouvesle, N., Kukui, A., and Le Bras, G.: Mechanism of the OH-
721 Initiated Oxidation of Glycolaldehyde over the Temperature Range 233–296 K, The
722 Journal of Physical Chemistry A, 110, 13492-13499, 10.1021/jp064993k, 2006a.

723 Butkovskaya, N. I., Pouvesle, N., Kukui, A., Mu, Y., and Le Bras, G.: Mechanism of
724 the OH-Initiated Oxidation of Hydroxyacetone over the Temperature Range 236–298

725 K, *The Journal of Physical Chemistry A*, 110, 6833-6843, 10.1021/jp056345r, 2006b.
726 Chandra, B. P. and Sinha, V.: Contribution of post-harvest agricultural paddy residue
727 fires in the N.W. Indo-Gangetic Plain to ambient carcinogenic benzenoids, toxic
728 isocyanic acid and carbon monoxide, *Environment International*, 88, 187-197,
729 10.1016/j.envint.2015.12.025, 2016.

730 Chebbi, A. and Carlier, P.: Carboxylic acids in the troposphere, occurrence, sources,
731 and sinks: A review, *Atmospheric Environment*, 30, 4233-4249,
732 [https://doi.org/10.1016/1352-2310\(96\)00102-1](https://doi.org/10.1016/1352-2310(96)00102-1), 1996.

733 Cope, J. D., Abellar, K. A., Bates, K. H., Fu, X., and Nguyen, T. B.: Aqueous
734 Photochemistry of 2-Methyltetrol and Erythritol as Sources of Formic Acid and
735 Acetic Acid in the Atmosphere, *ACS Earth and Space Chemistry*, 5, 1265-1277,
736 10.1021/acsearthspacechem.1c00107, 2021.

737 De Gouw, J. A., Gilman, J. B., Kim, S. W., Alvarez, S. L., Dusanter, S., Graus, M.,
738 Griffith, S. M., Isaacman - VanWertz, G., Kuster, W. C., Lefer, B. L., Lerner, B. M.,
739 McDonald, B. C., Rappenglück, B., Roberts, J. M., Stevens, P. S., Stutz, J., Thalman,
740 R., Veres, P. R., Volkamer, R., Warneke, C., Washenfelder, R. A., and Young, C. J.:
741 Chemistry of Volatile Organic Compounds in the Los Angeles Basin: Formation of
742 Oxygenated Compounds and Determination of Emission Ratios, *Journal of*
743 *Geophysical Research: Atmospheres*, 123, 2298-2319, 10.1002/2017jd027976, 2018.

744 Deming, B. L., Pagonis, D., Liu, X., Day, D. A., Talukdar, R., Krechmer, J. E., de Gouw,
745 J. A., Jimenez, J. L., and Ziemann, P. J.: Measurements of delays of gas-phase
746 compounds in a wide variety of tubing materials due to gas-wall interactions,
747 *Atmospheric Measurement Techniques*, 12, 3453-3461, 10.5194/amt-12-3453-2019,
748 2019.

749 Enders, G., Dlugi, R., Steinbrecher, R., Clement, B., Daiber, R., Eijk, J. v., Gäb, S.,
750 Haziza, M., Helas, G., Herrmann, U., Kessel, M., Kesselmeier, J., Kotzias, D.,
751 Kourtidis, K., Kurth, H. H., McMillen, R. T., Roeder, G., Schürmann, W., Teichmann,
752 U., and Torres, L.: Biosphere/Atmosphere interactions: Integrated research in a
753 European coniferous forest ecosystem, *Atmospheric Environment*, 26, 171-189,
754 [https://doi.org/10.1016/0960-1686\(92\)90269-Q](https://doi.org/10.1016/0960-1686(92)90269-Q), 1992.

755 Fang, X., Shao, M., Stohl, A., Zhang, Q., Zheng, J., Guo, H., Wang, C., Wang, M., Ou,
756 J., Thompson, R. L., and Prinn, R. G.: Top-down estimates of benzene and toluene
757 emissions in the Pearl River Delta and Hong Kong, China, *Atmospheric Chemistry*
758 *and Physics*, 16, 3369-3382, 10.5194/acp-16-3369-2016, 2016.

759 Franco, B., Blumenstock, T., Cho, C., Clarisse, L., Clerbaux, C., Coheur, P. F., De
760 Mazière, M., De Smedt, I., Dorn, H. P., Emmerichs, T., Fuchs, H., Gkatzelis, G.,
761 Griffith, D. W. T., Gromov, S., Hannigan, J. W., Hase, F., Hohaus, T., Jones, N.,
762 Kerkweg, A., Kiendler-Scharr, A., Lutsch, E., Mahieu, E., Novelli, A., Ortega, I.,
763 Paton-Walsh, C., Pommier, M., Pozzer, A., Reimer, D., Rosanka, S., Sander, R.,
764 Schneider, M., Strong, K., Tillmann, R., Van Roozendaal, M., Vereecken, L.,
765 Vigouroux, C., Wahner, A., and Taraborrelli, D.: Ubiquitous atmospheric production
766 of organic acids mediated by cloud droplets, *Nature*, 593, 233-237, 10.1038/s41586-

767 021-03462-x, 2021.

768 Fulgham, S. R., Brophy, P., Link, M., Ortega, J., Pollack, I., and Farmer, D. K.: Seasonal
769 Flux Measurements over a Colorado Pine Forest Demonstrate a Persistent Source of
770 Organic Acids, *ACS Earth and Space Chemistry*, 3, 2017-2032,
771 10.1021/acsearthspacechem.9b00182, 2019.

772 Galloway, J. N., Likens, G. E., Keene, W. C., and Miller, J. M.: The composition of
773 precipitation in remote areas of the world, *Journal of Geophysical Research: Oceans*,
774 87, 8771-8786, <https://doi.org/10.1029/JC087iC11p08771>, 1982.

775 Goode, J. G., Yokelson, R. J., Ward, D. E., Susott, R. A., Babbitt, R. E., Davies, M. A.,
776 and Hao, W. M.: Measurements of excess O₃, CO₂, CO, CH₄, C₂H₄, C₂H₂, HCN, NO,
777 NH₃, HCOOH, CH₃COOH, HCHO, and CH₃OH in 1997 Alaskan biomass burning
778 plumes by airborne Fourier transform infrared spectroscopy (AFTIR), *Journal of*
779 *Geophysical Research: Atmospheres*, 105, 22147-22166, 10.1029/2000jd900287,
780 2000.

781 Grosjean, D., Williams, E. L., II, and Grosjean, E.: Atmospheric chemistry of isoprene
782 and of its carbonyl products, *Environmental Science & Technology*, 27, 830-840,
783 10.1021/es00042a004, 1993.

784 Helmig, D., Johnson, B., Oltmans, S., Neff, W., Eisele, F., and Davis, D.: Elevated
785 ozone in the boundary layer at South Pole, *Atmospheric Environment*, 42, 2788-2803,
786 10.1016/j.atmosenv.2006.12.032, 2008a.

787 Helmig, D., Johnson, B., Warshawsky, M., Morse, T., Neff, W., Eisele, F., and Davis,
788 D.: Nitric oxide in the boundary-layer at South Pole during the Antarctic
789 Tropospheric Chemistry Investigation (ANTCI), *Atmospheric Environment*, 42,
790 2817-2830, 10.1016/j.atmosenv.2007.03.061, 2008b.

791 Hems, R. F., Wang, C., Collins, D. B., Zhou, S., Borduas-Dedekind, N., Siegel, J. A.,
792 and Abbatt, J. P. D.: Sources of isocyanic acid (HNCO) indoors: a focus on cigarette
793 smoke, *Environmental Science: Processes & Impacts*, 21, 1334-1341,
794 10.1039/c9em00107g, 2019.

795 Hu, L., Millet, D. B., Kim, S. Y., Wells, K. C., Griffis, T. J., Fischer, E. V., Helmig, D.,
796 Hueber, J., and Curtis, A. J.: North American acetone sources determined from tall
797 tower measurements and inverse modeling, *Atmospheric Chemistry and Physics*, 13,
798 3379-3392, 10.5194/acp-13-3379-2013, 2013.

799 Hu, X., Yang, G., Liu, Y., Lu, Y., Wang, Y., Chen, H., Chen, J., and Wang, L.:
800 Atmospheric gaseous organic acids in winter in a rural site of the North China Plain,
801 *Journal of Environmental Sciences*, 113, 190-203, 10.1016/j.jes.2021.05.035, 2022.

802 Jacob, D. J.: Chemistry of OH in remote clouds and its role in the production of formic
803 acid and peroxymonosulfate, *Journal of Geophysical Research: Atmospheres*, 91,
804 9807-9826, <https://doi.org/10.1029/JD091iD09p09807>, 1986.

805 Jaisson, S., Pietrement, C., and Gillery, P.: Carbamylation-derived products: bioactive
806 compounds and potential biomarkers in chronic renal failure and atherosclerosis,
807 *Clinical chemistry*, 57, 1499-1505, 10.1373/clinchem.2011.163188, 2011.

808 Jathar, S. H., Heppding, C., Link, M. F., Farmer, D. K., Akherati, A., Kleman, M. J.,

809 de Gouw, J. A., Veres, P. R., and Roberts, J. M.: Investigating diesel engines as an
810 atmospheric source of isocyanic acid in urban areas, *Atmospheric Chemistry and*
811 *Physics*, 17, 8959-8970, 10.5194/acp-17-8959-2017, 2017.

812 Ji, Y., Huey, L. G., Tanner, D. J., Lee, Y. R., Veres, P. R., Neuman, J. A., Wang, Y., and
813 Wang, X.: A vacuum ultraviolet ion source (VUV-IS) for iodide-chemical ionization
814 mass spectrometry: a substitute for radioactive ion sources, *Atmospheric*
815 *Measurement Techniques*, 13, 3683-3696, 10.5194/amt-13-3683-2020, 2020.

816 Karion, A., Sweeney, C., Tans, P., and Newberger, T.: AirCore: An Innovative
817 Atmospheric Sampling System, *Journal of Atmospheric and Oceanic Technology*, 27,
818 1839-1853, 10.1175/2010jtecha1448.1, 2010.

819 Kawamura, K. and Kaplan, I. R.: Organic compounds in the rainwater of Los Angeles,
820 *Environmental Science & Technology*, 17, 497-501, 10.1021/es00114a011, 1983.

821 Kawamura, K., Steinberg, S., and Kaplan, I. R.: Homologous series of C₁-C₁₀
822 monocarboxylic acids and C₁-C₆ carbonyls in Los Angeles air and motor vehicle
823 exhausts, *Atmospheric Environment*, 34, 4175-4191, [https://doi.org/10.1016/S1352-](https://doi.org/10.1016/S1352-2310(00)00212-0)
824 [2310\(00\)00212-0](https://doi.org/10.1016/S1352-2310(00)00212-0), 2000.

825 Keene, W. C. and Galloway, J. N.: Organic acidity in precipitation of North America,
826 *Atmospheric Environment*, 18, 2491-2497, [https://doi.org/10.1016/0004-](https://doi.org/10.1016/0004-6981(84)90020-9)
827 [6981\(84\)90020-9](https://doi.org/10.1016/0004-6981(84)90020-9), 1984.

828 Kesselmeier, J., Bode, K., Gerlach, C., and Jork, E. M.: Exchange of atmospheric
829 formic and acetic acids with trees and crop plants under controlled chamber and
830 purified air conditions, *Atmospheric Environment*, 32, 1765-1775,
831 [https://doi.org/10.1016/S1352-2310\(97\)00465-2](https://doi.org/10.1016/S1352-2310(97)00465-2), 1998.

832 Khare, P., Kumar, N., Kumari, K. M., and Srivastava, S. S.: Atmospheric formic and
833 acetic acids: An overview, *Reviews of Geophysics*, 37, 227-248,
834 <https://doi.org/10.1029/1998RG900005>, 1999.

835 Koeth, R. A., Kalantar-Zadeh, K., Wang, Z., Fu, X., Tang, W. H., and Hazen, S. L.:
836 Protein carbamylation predicts mortality in ESRD, *Journal of the American Society*
837 *of Nephrology*, 24, 853-861, 10.1681/ASN.2012030254, 2013.

838 Krechmer, J. E., Day, D. A., Ziemann, P. J., and Jimenez, J. L.: Direct Measurements
839 of Gas/Particle Partitioning and Mass Accommodation Coefficients in
840 Environmental Chambers, *Environmental science & technology*, 51, 11867-11875,
841 10.1021/acs.est.7b02144, 2017.

842 Le Breton, M., Bacak, A., Muller, J. B. A., Xiao, P., Shallcross, B. M. A., Batt, R.,
843 Cooke, M. C., Shallcross, D. E., Bauguitte, S. J. B., and Percival, C. J.: Simultaneous
844 airborne nitric acid and formic acid measurements using a chemical ionization mass
845 spectrometer around the UK: Analysis of primary and secondary production
846 pathways, *Atmospheric Environment*, 83, 166-175, 10.1016/j.atmosenv.2013.10.008,
847 2014.

848 Lei, X., Wang, W., Gao, J., Wang, S., and Wang, W.: Atmospheric Chemistry of Enols:
849 The Formation Mechanisms of Formic and Peroxyformic Acids in Ozonolysis of
850 Vinyl Alcohol, *The Journal of Physical Chemistry A*, 124, 4271-4279,

851 10.1021/acs.jpca.0c01480, 2020.

852 Li, T., Wang, Z., Yuan, B., Ye, C., Lin, Y., Wang, S., Sha, Q. e., Yuan, Z., Zheng, J., and
853 Shao, M.: Emissions of carboxylic acids, hydrogen cyanide (HCN) and isocyanic
854 acid (HNCO) from vehicle exhaust, *Atmospheric Environment*, 247,
855 10.1016/j.atmosenv.2021.118218, 2021.

856 Li, X.-B., Yuan, B., Wang, S., Wang, C., Lan, J., Liu, Z., Song, Y., He, X., Huangfu, Y.,
857 Pei, C., Cheng, P., Yang, S., Qi, J., Wu, C., Huang, S., You, Y., Chang, M., Zheng, H.,
858 Yang, W., Wang, X., and Shao, M.: Variations and sources of volatile organic
859 compounds (VOCs) in urban region: insights from measurements on a tall tower,
860 *Atmospheric Chemistry and Physics*, 22, 10567-10587, 10.5194/acp-22-10567-2022,
861 2022.

862 Li, X., Zhang, C., Liu, A., Yuan, B., Yang, H., Liu, C., Wang, S., Huangfu, Y., Qi, J.,
863 Liu, Z., He, X., Song, X., Chen, Y., Peng, Y., Zhang, X., Zheng, E., Yang, L., Yang,
864 Q., Qin, G., Zhou, J., and Shao, M.: Assessment of Long Tubing in Measuring
865 Atmospheric Trace Gases: Applications on Tall Towers, *Environmental Science:
866 Atmospheres*, 506-520, 10.1039/d2ea00110a, 2023.

867 Liggio, J., Moussa, S. G., Wentzell, J., Darlington, A., Liu, P., Leithead, A., Hayden, K.,
868 O'Brien, J., Mittermeier, R. L., Staebler, R., Wolde, M., and Li, S.-M.: Understanding
869 the primary emissions and secondary formation of gaseous organic acids in the oil
870 sands region of Alberta, Canada, *Atmospheric Chemistry and Physics*, 17, 8411-8427,
871 10.5194/acp-17-8411-2017, 2017.

872 Link, M. F., Brophy, P., Fulgham, S. R., Murschell, T., and Farmer, D. K.: Isoprene
873 versus Monoterpenes as Gas-Phase Organic Acid Precursors in the Atmosphere, *ACS
874 Earth and Space Chemistry*, 5, 1600-1612, 10.1021/acsearthspacechem.1c00093,
875 2021.

876 Link, M. F., Nguyen, T. B., Bates, K., Müller, J.-F., and Farmer, D. K.: Can Isoprene
877 Oxidation Explain High Concentrations of Atmospheric Formic and Acetic Acid over
878 Forests?, *ACS Earth and Space Chemistry*, 4, 730-740,
879 10.1021/acsearthspacechem.0c00010, 2020.

880 Liu, X., Deming, B., Pagonis, D., Day, D. A., Palm, B. B., Talukdar, R., Roberts, J. M.,
881 Veres, P. R., Krechmer, J. E., Thornton, J. A., de Gouw, J. A., Ziemann, P. J., and
882 Jimenez, J. L.: Effects of gas-wall interactions on measurements of semivolatile
883 compounds and small polar molecules, *Atmospheric Measurement Techniques*, 12,
884 3137-3149, 10.5194/amt-12-3137-2019, 2019.

885 Lopez-Hilfiker, F. D., Mohr, C., Ehn, M., Rubach, F., Kleist, E., Wildt, J., Mentel, T. F.,
886 Lutz, A., Hallquist, M., Worsnop, D., and Thornton, J. A.: A novel method for online
887 analysis of gas and particle composition: description and evaluation of a Filter Inlet
888 for Gases and AEROSols (FIGAERO), *Atmospheric Measurement Techniques*, 7,
889 983-1001, 10.5194/amt-7-983-2014, 2014.

890 Mattila, J. M., Brophy, P., Kirkland, J., Hall, S., Ullmann, K., Fischer, E. V., Brown, S.,
891 McDuffie, E., Tevlin, A., and Farmer, D. K.: Tropospheric sources and sinks of gas-
892 phase acids in the Colorado Front Range, *Atmospheric Chemistry and Physics*, 18,

893 12315-12327, 10.5194/acp-18-12315-2018, 2018.

894 Meng, F., Qin, M., Tang, K., Duan, J., Fang, W., Liang, S., Ye, K., Xie, P., Sun, Y., Xie,
895 C., Ye, C., Fu, P., Liu, J., and Liu, W.: High-resolution vertical distribution and
896 sources of HONO and NO₂ in the nocturnal boundary layer in urban Beijing, China,
897 Atmospheric Chemistry and Physics, 20, 5071-5092, 10.5194/acp-20-5071-2020,
898 2020.

899 Millet, D. B., Baasandorj, M., Farmer, D. K., Thornton, J. A., Baumann, K., Brophy, P.,
900 Chaliyakunnel, S., de Gouw, J. A., Graus, M., Hu, L., Koss, A., Lee, B. H., Lopez-
901 Hilfiker, F. D., Neuman, J. A., Paulot, F., Peischl, J., Pollack, I. B., Ryerson, T. B.,
902 Warneke, C., Williams, B. J., and Xu, J.: A large and ubiquitous source of
903 atmospheric formic acid, Atmospheric Chemistry and Physics, 15, 6283-6304,
904 10.5194/acp-15-6283-2015, 2015.

905 Mungall, E. L., Abbatt, J. P. D., Wentzell, J. J. B., Wentworth, G. R., Murphy, J. G.,
906 Kunkel, D., Gute, E., Tarasick, D. W., Sharma, S., Cox, C. J., Uttal, T., and Liggio,
907 J.: High gas-phase mixing ratios of formic and acetic acid in the High Arctic,
908 Atmospheric Chemistry and Physics, 18, 10237-10254, 10.5194/acp-18-10237-2018,
909 2018.

910 Mydel, P., Wang, Z., Brisslert, M., Hellvard, A., Dahlberg, L. E., Hazen, S. L., and
911 Bokarewa, M. I. J. T. J. o. I.: Carbamylation-Dependent Activation of T Cells: A
912 Novel Mechanism in the Pathogenesis of Autoimmune Arthritis, The Journal of
913 Immunology, 184, 6882 - 6890, 2010.

914 Neeb, P., Sauer, F., Horie, O., and Moortgat, G. K.: Formation of hydroxymethyl
915 hydroperoxide and formic acid in alkene ozonolysis in the presence of water vapour,
916 Atmospheric Environment, 31, 1417-1423, [https://doi.org/10.1016/S1352-
917 2310\(96\)00322-6](https://doi.org/10.1016/S1352-2310(96)00322-6), 1997.

918 Pagonis, D., Krechmer, J. E., de Gouw, J., Jimenez, J. L., and Ziemann, P. J.: Effects of
919 gas-wall partitioning in Teflon tubing and instrumentation on time-resolved
920 measurements of gas-phase organic compounds, Atmospheric Measurement
921 Techniques, 10, 4687-4696, 10.5194/amt-10-4687-2017, 2017.

922 Palm, B. B., Liu, X., Jimenez, J. L., and Thornton, J. A.: Performance of a new coaxial
923 ion-molecule reaction region for low-pressure chemical ionization mass
924 spectrometry with reduced instrument wall interactions, Atmospheric Measurement
925 Techniques, 12, 5829-5844, 10.5194/amt-12-5829-2019, 2019.

926 Paulot, F., Crouse, J. D., Kjaergaard, H. G., Kroll, J. H., Seinfeld, J. H., and Wennberg,
927 P. O.: Isoprene photooxidation: new insights into the production of acids and organic
928 nitrates, Atmospheric Chemistry and Physics, 9, 1479-1501, 10.5194/acp-9-1479-
929 2009, 2009.

930 Paulot, F., Wunch, D., Crouse, J. D., Toon, G. C., Millet, D. B., DeCarlo, P. F.,
931 Vigouroux, C., Deutscher, N. M., Gonzalez Abad, G., Notholt, J., Warneke, T.,
932 Hannigan, J. W., Warneke, C., de Gouw, J. A., Dunlea, E. J., De Maziere, M., Griffith,
933 D. W. T., Bernath, P., Jimenez, J. L., and Wennberg, P. O.: Importance of secondary
934 sources in the atmospheric budgets of formic and acetic acids, Atmospheric

935 Chemistry and Physics, 11, 1989-2013, 10.5194/acp-11-1989-2011, 2011.

936 Roberts, J. M. and Liu, Y.: Solubility and solution-phase chemistry of isocyanic acid,
937 methyl isocyanate, and cyanogen halides, *Atmospheric Chemistry and Physics*, 19,
938 4419-4437, 10.5194/acp-19-4419-2019, 2019.

939 Roberts, J. M., Veres, P. R., Cochran, A. K., Warneke, C., Burling, I. R., Yokelson, R.
940 J., Lerner, B., Gilman, J. B., Kuster, W. C., Fall, R., and de Gouw, J.: Isocyanic acid
941 in the atmosphere and its possible link to smoke-related health effects, *Proceedings*
942 *of the National Academy of Sciences*, 108, 8966-8971, 10.1073/pnas.1103352108,
943 2011.

944 Roberts, J. M., Veres, P. R., VandenBoer, T. C., Warneke, C., Graus, M., Williams, E.
945 J., Lefer, B., Brock, C. A., Bahreini, R., Öztürk, F., Middlebrook, A. M., Wagner, N.
946 L., Dubé, W. P., and de Gouw, J. A.: New insights into atmospheric sources and sinks
947 of isocyanic acid, HNCO, from recent urban and regional observations, *Journal of*
948 *Geophysical Research: Atmospheres*, 119, 1060-1072, 10.1002/2013jd019931, 2014.

949 Rosanka, S., Vu, G. H. T., Nguyen, H. M. T., Pham, T. V., Javed, U., Taraborrelli, D.,
950 and Vereecken, L.: Atmospheric chemical loss processes of isocyanic acid (HNCO):
951 a combined theoretical kinetic and global modelling study, *Atmospheric Chemistry*
952 *and Physics*, 20, 6671-6686, 10.5194/acp-20-6671-2020, 2020.

953 Schnitzhofer, R., Wisthaler, A., and Hansel, A.: Real-time profiling of organic trace
954 gases in the planetary boundary layer by PTR-MS using a tethered balloon,
955 *Atmospheric Measurement Techniques*, 2, 773-777, 10.5194/amt-2-773-2009, 2009.

956 Schobesberger, S., Lopez - Hilfiker, F. D., Taipale, D., Millet, D. B., D'Ambro, E. L.,
957 Rantala, P., Mammarella, I., Zhou, P., Wolfe, G. M., Lee, B. H., Boy, M., and
958 Thornton, J. A.: High upward fluxes of formic acid from a boreal forest canopy,
959 *Geophysical Research Letters*, 43, 9342-9351, 10.1002/2016gl069599, 2016.

960 Skorokhod, A. I., Berezina, E. V., Moiseenko, K. B., Elansky, N. F., and Belikov, I. B.:
961 Benzene and toluene in the surface air of northern Eurasia from TROICA-12
962 campaign along the Trans-Siberian Railway, *Atmospheric Chemistry and Physics*, 17,
963 5501-5514, 10.5194/acp-17-5501-2017, 2017.

964 Stavrou, T., Müller, J. F., Peeters, J., Razavi, A., Clarisse, L., Clerbaux, C., Coheur,
965 P. F., Hurtmans, D., De Mazière, M., Vigouroux, C., Deutscher, N. M., Griffith, D.
966 W. T., Jones, N., and Paton-Walsh, C.: Satellite evidence for a large source of formic
967 acid from boreal and tropical forests, *Nature Geoscience*, 5, 26-30,
968 10.1038/ngeo1354, 2011.

969 Tan, Q., Ge, B., Xu, X., Gan, L., Yang, W., Chen, X., Pan, X., Wang, W., Li, J., and
970 Wang, Z.: Increasing impacts of the relative contributions of regional transport on air
971 pollution in Beijing: Observational evidence, *Environmental Pollution*, 292, 118407,
972 10.1016/j.envpol.2021.118407, 2022.

973 Verbrugge, F. H., Tang, W. H., and Hazen, S. L.: Protein carbamylation and
974 cardiovascular disease, *Kidney International*, 88, 474-478, 10.1038/ki.2015.166,
975 2015.

976 Veres, P. R., Roberts, J. M., Cochran, A. K., Gilman, J. B., Kuster, W. C., Holloway, J.

977 S., Graus, M., Flynn, J., Lefer, B., Warneke, C., and de Gouw, J.: Evidence of rapid
978 production of organic acids in an urban air mass, *Geophysical Research Letters*, 38,
979 L17807, 10.1029/2011gl048420, 2011.

980 Wang, Z., Nicholls, S. J., Rodriguez, E. R., Kummu, O., Horkko, S., Barnard, J.,
981 Reynolds, W. F., Topol, E. J., DiDonato, J. A., and Hazen, S. L.: Protein
982 carbamylation links inflammation, smoking, uremia and atherogenesis, *Nature*
983 *medicine*, 13, 1176-1184, 10.1038/nm1637, 2007.

984 Wang, Z., Yuan, B., Ye, C., Roberts, J., Wisthaler, A., Lin, Y., Li, T., Wu, C., Peng, Y.,
985 Wang, C., Wang, S., Yang, S., Wang, B., Qi, J., Wang, C., Song, W., Hu, W., Wang,
986 X., Xu, W., Ma, N., Kuang, Y., Tao, J., Zhang, Z., Su, H., Cheng, Y., Wang, X., and
987 Shao, M.: High Concentrations of Atmospheric Isocyanic Acid (HNCO) Produced
988 from Secondary Sources in China, *Environmental Science & Technology*, 54, 11818-
989 11826, 10.1021/acs.est.0c02843, 2020.

990 Wentzell, J. J., Liggio, J., Li, S. M., Vlasenko, A., Staebler, R., Lu, G., Poitras, M. J.,
991 Chan, T., and Brook, J. R.: Measurements of gas phase acids in diesel exhaust: a
992 relevant source of HNCO?, *Environmental Science & Technology*, 47, 7663-7671,
993 10.1021/es401127j, 2013.

994 Woodward-Massey, R., Taha, Y. M., Moussa, S. G., and Osthoff, H. D.: Comparison of
995 negative-ion proton-transfer with iodide ion chemical ionization mass spectrometry
996 for quantification of isocyanic acid in ambient air, *Atmospheric Environment*, 98,
997 693-703, 10.1016/j.atmosenv.2014.09.014, 2014.

998 Wren, S. N., Liggio, J., Han, Y., Hayden, K., Lu, G., Mihele, C. M., Mittermeier, R. L.,
999 Stroud, C., Wentzell, J. J. B., and Brook, J. R.: Elucidating real-world vehicle
1000 emission factors from mobile measurements over a large metropolitan region: a focus
1001 on isocyanic acid, hydrogen cyanide, and black carbon, *Atmospheric Chemistry and*
1002 *Physics*, 18, 16979-17001, 10.5194/acp-18-16979-2018, 2018.

1003 Wu, C., Wang, C., Wang, S., Wang, W., Yuan, B., Qi, J., Wang, B., Wang, H., Wang, C.,
1004 Song, W., Wang, X., Hu, W., Lou, S., Ye, C., Peng, Y., Wang, Z., Huangfu, Y., Xie,
1005 Y., Zhu, M., Zheng, J., Wang, X., Jiang, B., Zhang, Z., and Shao, M.: Measurement
1006 report: Important contributions of oxygenated compounds to emissions and
1007 chemistry of volatile organic compounds in urban air, *Atmos. Chem. Phys.*, 20,
1008 14769-14785, <https://doi.org/10.5194/acp-20-14769-2020>, 2020.

1009 Yan, Y., Wang, S., Zhu, J., Guo, Y., Tang, G., Liu, B., An, X., Wang, Y., and Zhou, B.:
1010 Vertically increased NO₃ radical in the nocturnal boundary layer, *Science of The*
1011 *Total Environment*, 763, 142969, <https://doi.org/10.1016/j.scitotenv.2020.142969>,
1012 2021.

1013 Yáñez-Serrano, A. M., Nölscher, A. C., Bourtsoukidis, E., Gomes Alves, E., Ganzeveld,
1014 L., Bonn, B., Wolff, S., Sa, M., Yamasoe, M., Williams, J., Andreae, M. O., and
1015 Kesselmeier, J.: Monoterpene chemical speciation in a tropical rainforest: variation
1016 with season, height, and time of day at the Amazon Tall Tower Observatory (ATTO),
1017 *Atmospheric Chemistry and Physics*, 18, 3403-3418, 10.5194/acp-18-3403-2018,
1018 2018.

1019 Yao, L., Wang, M. Y., Wang, X. K., Liu, Y. J., Chen, H. F., Zheng, J., Nie, W., Ding, A.
1020 J., Geng, F. H., Wang, D. F., Chen, J. M., Worsnop, D. R., and Wang, L.: Detection
1021 of atmospheric gaseous amines and amides by a high-resolution time-of-flight
1022 chemical ionization mass spectrometer with protonated ethanol reagent ions,
1023 *Atmospheric Chemistry and Physics*, 16, 14527-14543, 10.5194/acp-16-14527-2016,
1024 2016.

1025 Yu, S.: Role of organic acids (formic, acetic, pyruvic and oxalic) in the formation of
1026 cloud condensation nuclei (CCN): a review, *Atmospheric Research*, 53, 185-217,
1027 [https://doi.org/10.1016/S0169-8095\(00\)00037-5](https://doi.org/10.1016/S0169-8095(00)00037-5), 2000.

1028 Yuan, B., Koss, A. R., Warneke, C., Coggon, M., Sekimoto, K., and de Gouw, J. A.:
1029 Proton-Transfer-Reaction Mass Spectrometry: Applications in Atmospheric Sciences,
1030 *Chemical reviews*, 117, 13187-13229, 10.1021/acs.chemrev.7b00325, 2017.

1031 Yuan, B., Shao, M., de Gouw, J., Parrish, D. D., Lu, S., Wang, M., Zeng, L., Zhang, Q.,
1032 Song, Y., Zhang, J., and Hu, M.: Volatile organic compounds (VOCs) in urban air:
1033 How chemistry affects the interpretation of positive matrix factorization (PMF)
1034 analysis, *Journal of Geophysical Research: Atmospheres*, 117, n/a-n/a,
1035 10.1029/2012jd018236, 2012.

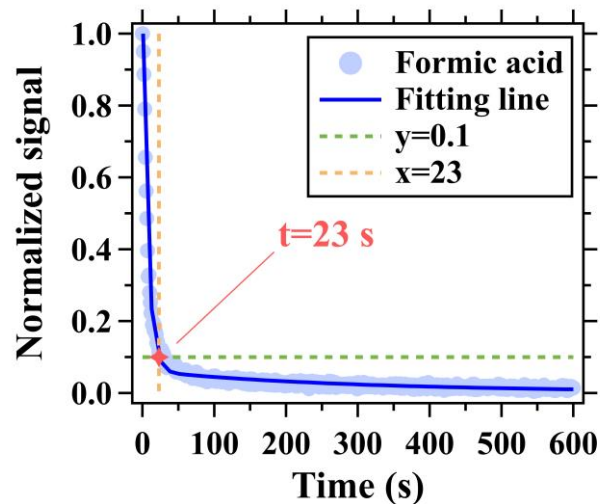
1036 Yuan, B., Veres, P. R., Warneke, C., Roberts, J. M., Gilman, J. B., Koss, A., Edwards,
1037 P. M., Graus, M., Kuster, W. C., Li, S. M., Wild, R. J., Brown, S. S., Dubé, W. P.,
1038 Lerner, B. M., Williams, E. J., Johnson, J. E., Quinn, P. K., Bates, T. S., Lefer, B.,
1039 Hayes, P. L., Jimenez, J. L., Weber, R. J., Zamora, R., Ervens, B., Millet, D. B.,
1040 Rappenglück, B., and de Gouw, J. A.: Investigation of secondary formation of formic
1041 acid: urban environment vs. oil and gas producing region, *Atmospheric Chemistry
1042 and Physics*, 15, 1975-1993, 10.5194/acp-15-1975-2015, 2015.

1043 Zhao, R., Yin, B., Zhang, N., Wang, J., Geng, C., Wang, X., Han, B., Li, K., Li, P., Yu,
1044 H., Yang, W., and Bai, Z.: Aircraft-based observation of gaseous pollutants in the
1045 lower troposphere over the Beijing-Tianjin-Hebei region, *Science of The Total
1046 Environment*, 773, 144818, 10.1016/j.scitotenv.2020.144818, 2021.

1047 Zhao, R., Lee, A. K. Y., Wentzell, J. J. B., McDonald, A. M., Toom-Saunty, D., Leaitch,
1048 W. R., Modini, R. L., Corrigan, A. L., Russell, L. M., Noone, K. J., Schroder, J. C.,
1049 Bertram, A. K., Hawkins, L. N., Abbatt, J. P. D., and Liggio, J.: Cloud partitioning
1050 of isocyanic acid (HNCO) and evidence of secondary source of HNCO in ambient
1051 air, *Geophysical Research Letters*, 41, 6962-6969, 10.1002/2014gl061112, 2014.

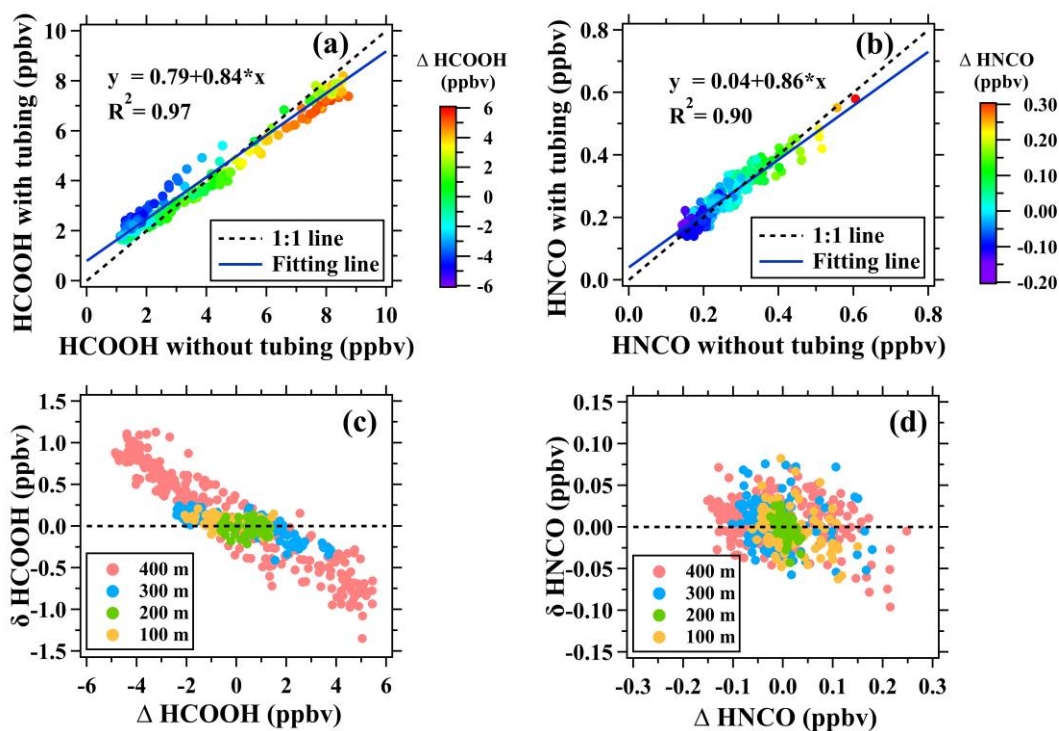
1052 Zhu, B., Han, Y., Wang, C., Huang, X., Xia, S., Niu, Y., Yin, Z., and He, L.:
1053 Understanding primary and secondary sources of ambient oxygenated volatile
1054 organic compounds in Shenzhen utilizing photochemical age-based parameterization
1055 method, *Journal of Environmental Sciences (China)*, 75, 105-114,
1056 10.1016/j.jes.2018.03.008, 2019.

1057



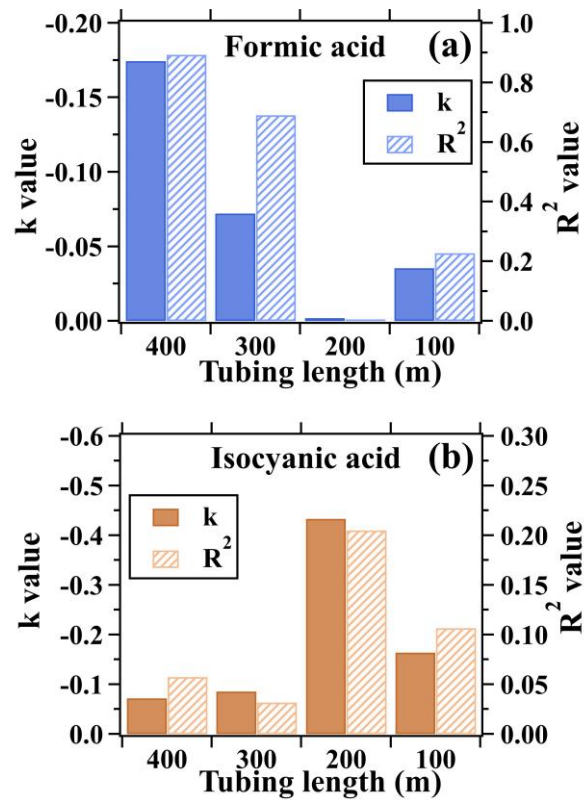
1058

1059 **Figure 1.** Depassivation curves of formic acid signal measured by I^- ToF-CIMS for the
 1060 400 m long tubing at the flow rate of 13 SLPM. Ion signals were normalized to those
 1061 measured at the start time (0 s) of the step-function change.



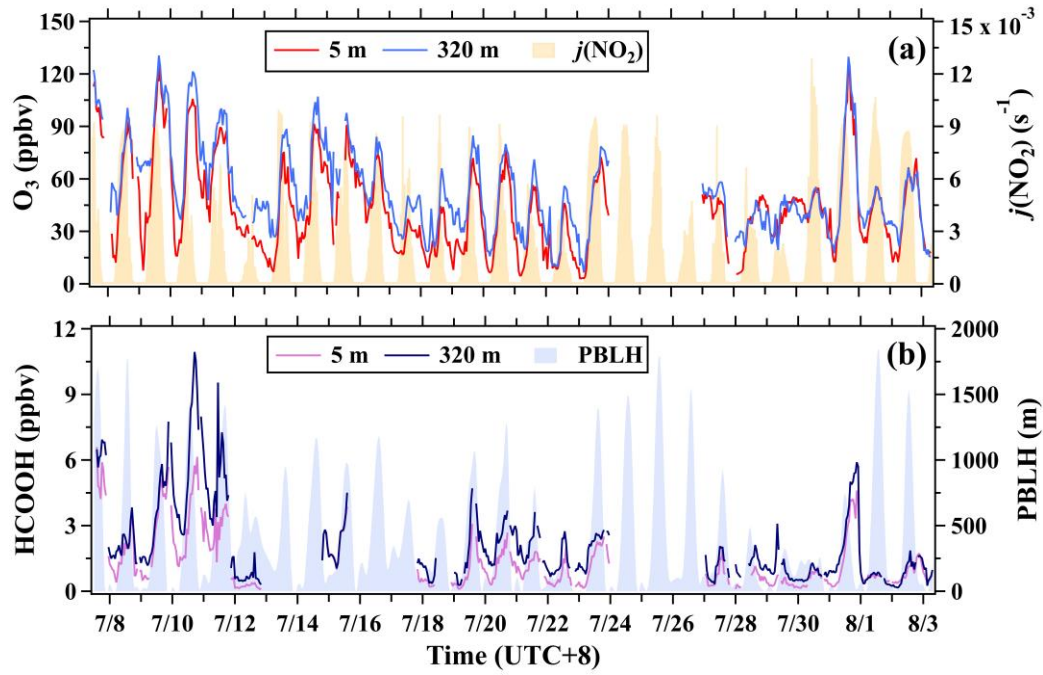
1062

1063 **Figure 2.** Assessment of long tubes in measuring formic and isocyanic acids in ambient
 1064 air. (a-b) Scatterplots of mixing ratios of formic and isocyanic acids measured with the
 1065 400 m long tube versus those measured without the long tube. (c-d) Scatterplots of
 1066 $\Delta[HCOOH]$ versus $\delta[HCOOH]$ and scatterplots of $\Delta[HNCO]$ versus $\delta[HNCO]$ for
 1067 the 100, 200, 300, and 400 m tubes.



1068

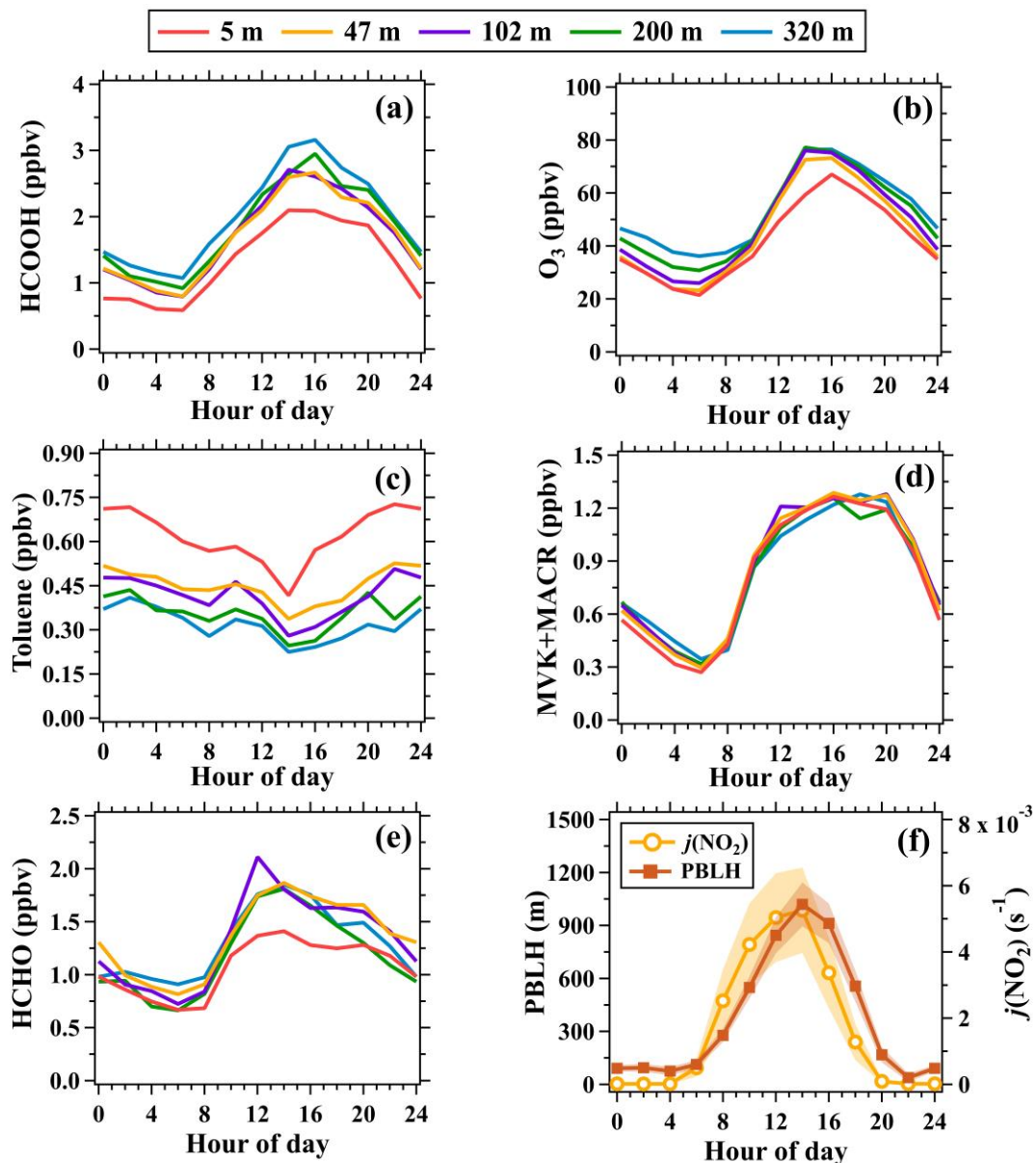
1069 **Figure 3.** Linear fitting parameters (namely k and R^2) for (a) $\Delta[HCOOH]$ versus
 1070 $\delta[HCOOH]$ and (b) $\Delta[HNCO]$ versus $\delta[HNCO]$. The scatterplots are shown in
 1071 Figure 2. k and R^2 are the slope and determination coefficient of the linear fitting lines,
 1072 respectively.



1073

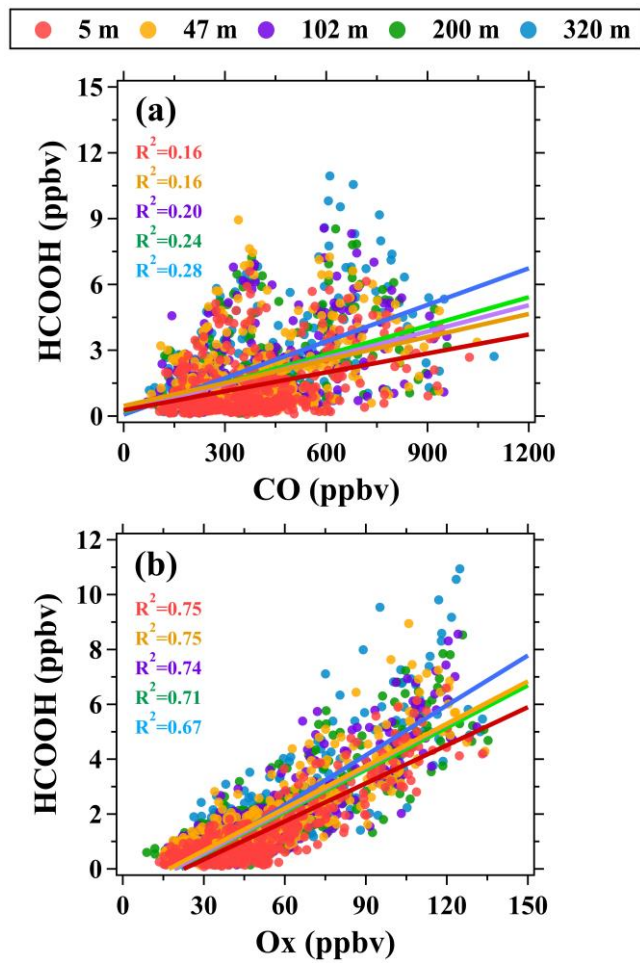
1074 **Figure 4.** Time series of (a) O₃ (5 and 320 m), $j(\text{NO}_2)$, (b) formic acid (5 and 320 m),

1075 and planetary boundary layer height (PBLH) during the campaign.



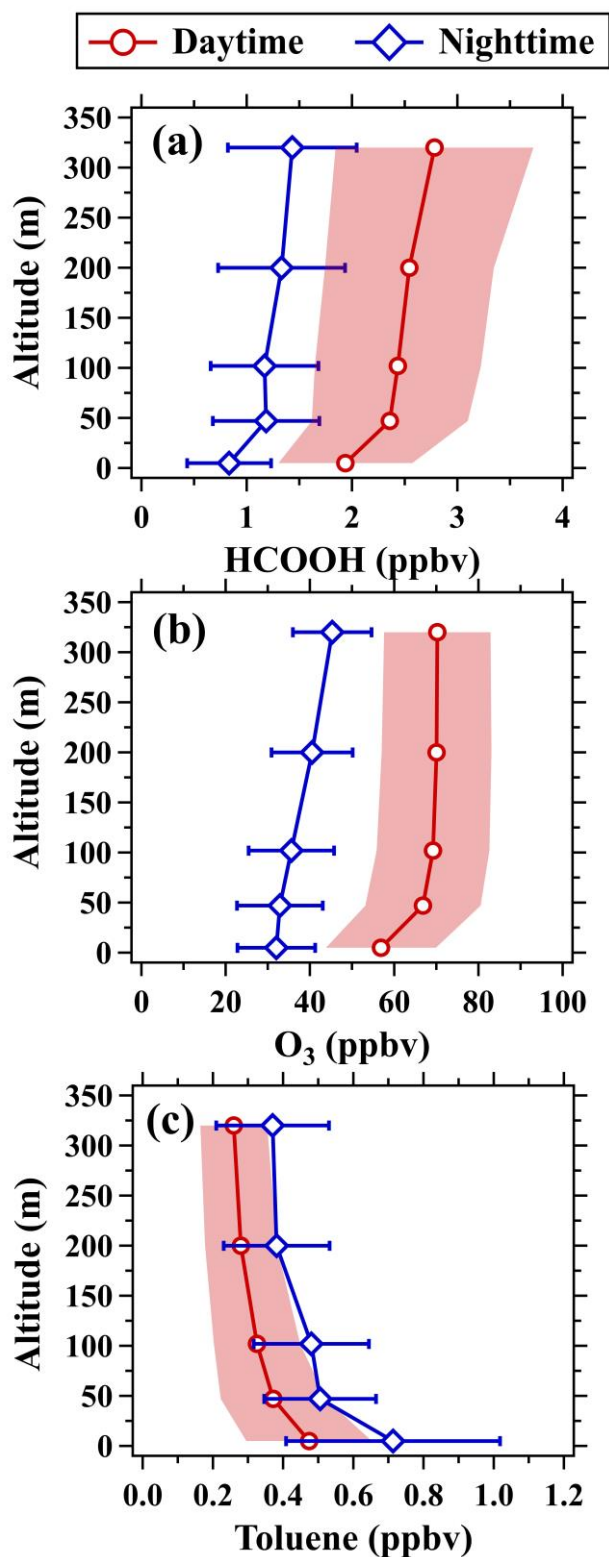
1076

1077 **Figure 5.** Average diurnal variations in mixing ratios of (a) formic acid, (b) O₃, (c)
 1078 toluene, (d) MVK+MACR, (e) formaldehyde at the five inlet heights and (f) PBLH and
 1079 $j(\text{NO}_2)$. The shaded areas in panel (f) are half of the standard deviations.



1080

1081 **Figure 6.** Scatter plots of (a) formic acid versus CO and (b) formic acid versus Ox at
 1082 different altitudes during the campaign.

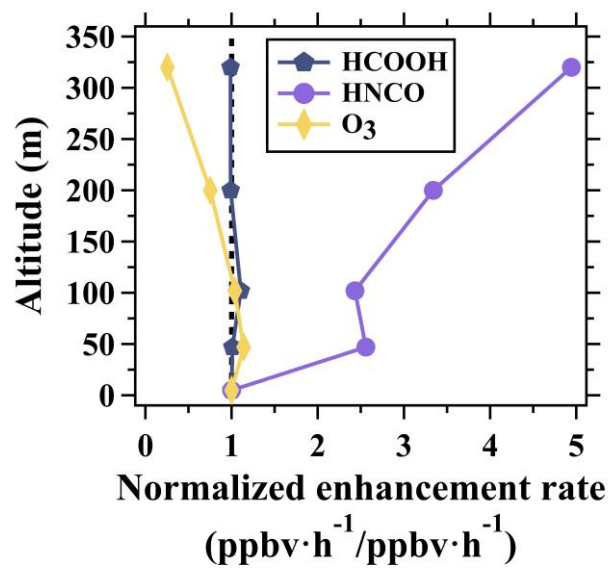


1083

1084 **Figure 7.** Vertical profiles of (a) formic acid, (b) O₃, and (c) toluene in daytime (11:00-

1085 16:00 LT) and nighttime (22:00-5:00 LT). The shaded areas and error bars are half of

1086 the standard deviations.



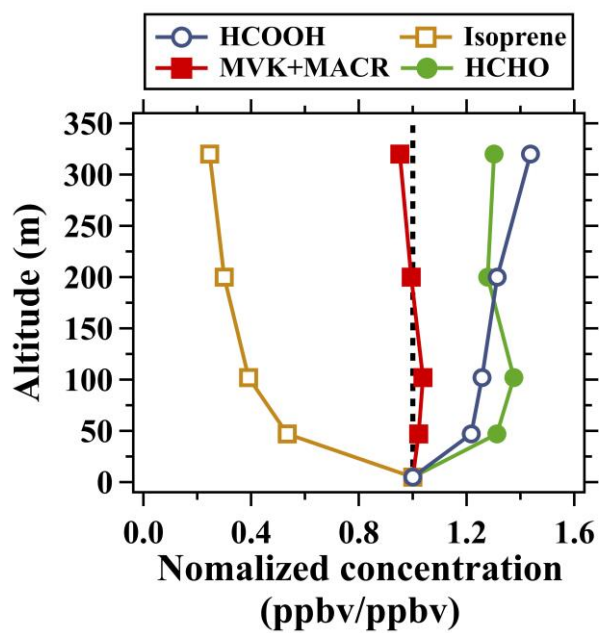
1087

1088 **Figure 8.** Normalized vertical profiles of the enhancement rate of ozone, formic acid,

1089 and isocyanic acid between 6:00-10:00 LT averaged over the whole campaign.

1090 Enhancement rate of the species at different altitudes were normalized to those at 5 m.

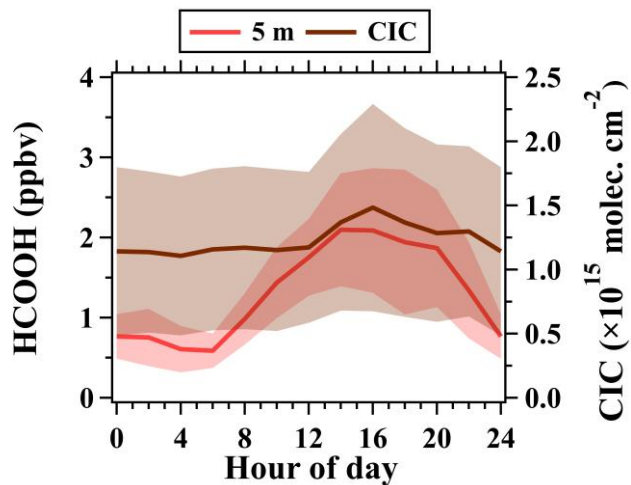
1091 The dotted line indicates the normalized enhancement rate of 1.



1092

1093 **Figure 9.** Normalized vertical profiles of formic acid, isoprene, formaldehyde, MVK
 1094 and MACR in daytime (11:00-16:00 LT) averaged over the whole campaign. Mixing
 1095 ratios of the species at different altitudes were normalized to those at 5 m. The dotted
 1096 line indicates the normalized concentration of 1.

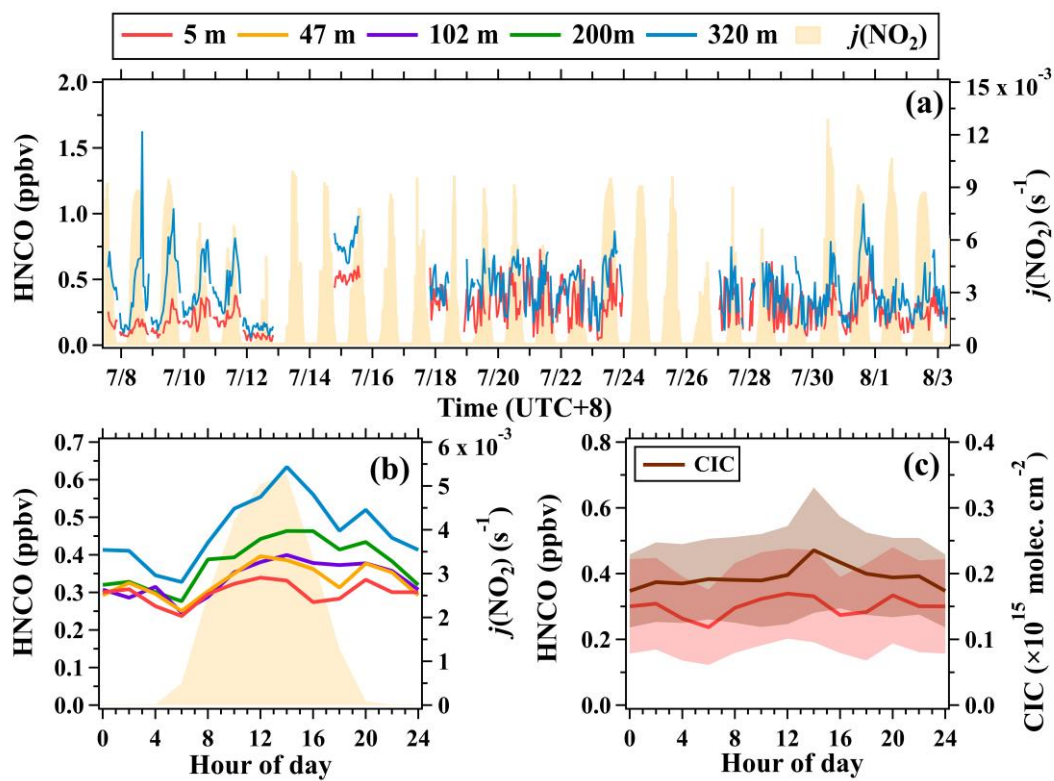
1097



1098

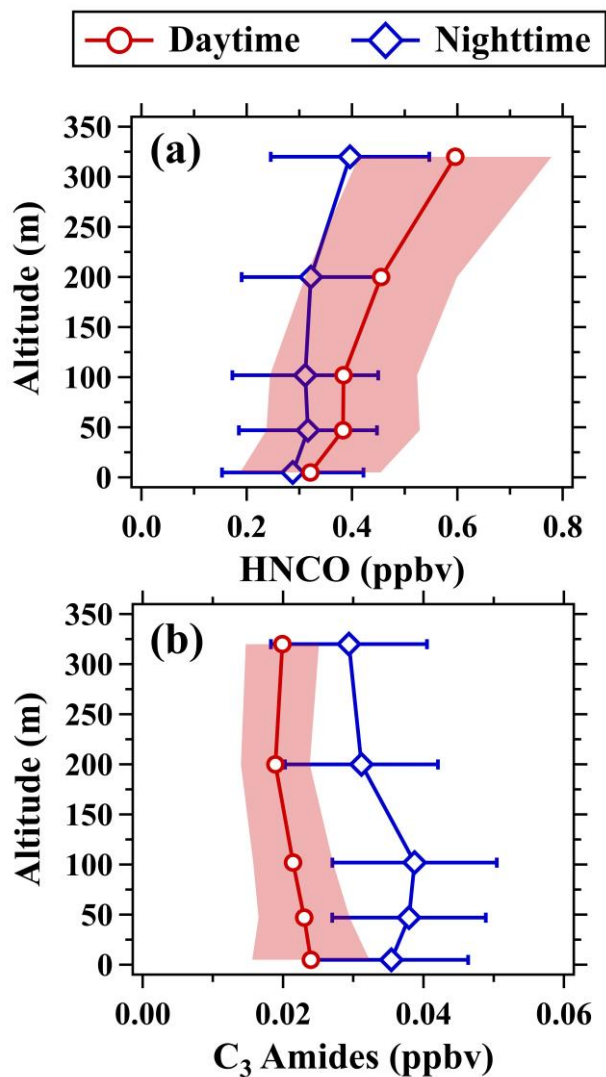
1099 **Figure 10.** Average diurnal variations in mixing ratios (5 m) and CICs of formic acid

1100 during the field campaign; The shaded areas are half of the standard deviations.

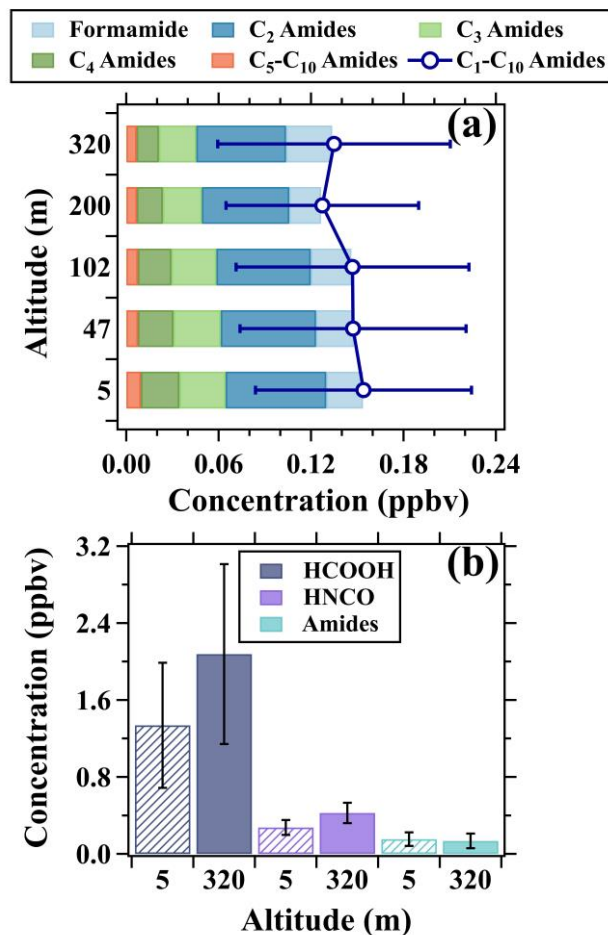


1101

1102 **Figure 11.** (a) Time series of isocyanic acid (5 and 320 m) and $j(\text{NO}_2)$. (b) Average
 1103 diurnal variations in isocyanic acid at 5, 47, 102, 200, and 320 m. (c) Average diurnal
 1104 variations in mixing ratios (5 m) and CICs of isocyanic acid during the campaign; The
 1105 shaded areas in panel (c) are half of the standard deviations.



1106
 1107 **Figure 12.** Vertical profiles of (a) isocyanic acid and (b) C₃ amides in daytime (11:00-
 1108 16:00 LT) and nighttime (22:00-5:00 LT). The shaded areas and error bars are half of
 1109 the standard deviations.
 1110



1111

1112 **Figure 13.** (a) Vertical variations in composition and concentrations of amides. (b)
 1113 Concentration comparison of formic acid, isocyanic acid, and amides between 5 and
 1114 320 m. The data in both (a) and (b) was the average results of the whole campaign. The
 1115 patterns of the bars are used to distinguish the average concentration of the species at
 1116 the two heights.